AD-A087 579 VISIDYNE INC BURLINGTON MASS F/G 4/1
EVALUATION AND DEVELOPMENT OF ADVANCED HIGH ALTITUDE EXPERIMENT--ETC(U)
DEC 78 J W CARPENTER, C HUMPHREY, A HURD F-19628-76-C-0198
UNCLASSIFIED VI-465 AFGL-TR-79-0043 NL

1 OF 1
AD
A087579

END
DATE FILMED
9-80
DTIC

AFGL-TR-79-0043

LEVEL II

EVALUATION AND DEVELOPMENT OF ADVANCED HIGH ALTITUDE EXPERIMENTS AND SYSTEMS

J.W. Carpenter
C.H. Humphrey
A.G. Hurd
W.P. Reidy
O. Shepherd
H.J.P. Smith
T.F. Zehnpfennig

Visidyne, Inc.
19 Third Avenue
Northwest Industrial Park
Burlington, Massachusetts 01803

1 December 1978

Final Report for the Period 15 May 1976 - 1 December 1978

Approved for Public Release; Distribution Unlimited

This work was sponsored in part by the Defense Nuclear Agency (DNA) and the Space Missile Systems Organization (SAMSO), and the contract work was conducted under the technical cognizance of the Air Force Geophysics Laboratory (AFGL), AFSC.

AIR FORCE GEOPHYSICS LABORATORY
AIR FORCE SYSTEMS COMMAND
UNITED STATES AIR FORCE
HANSCOM AFB, MASSACHUSETTS 01731

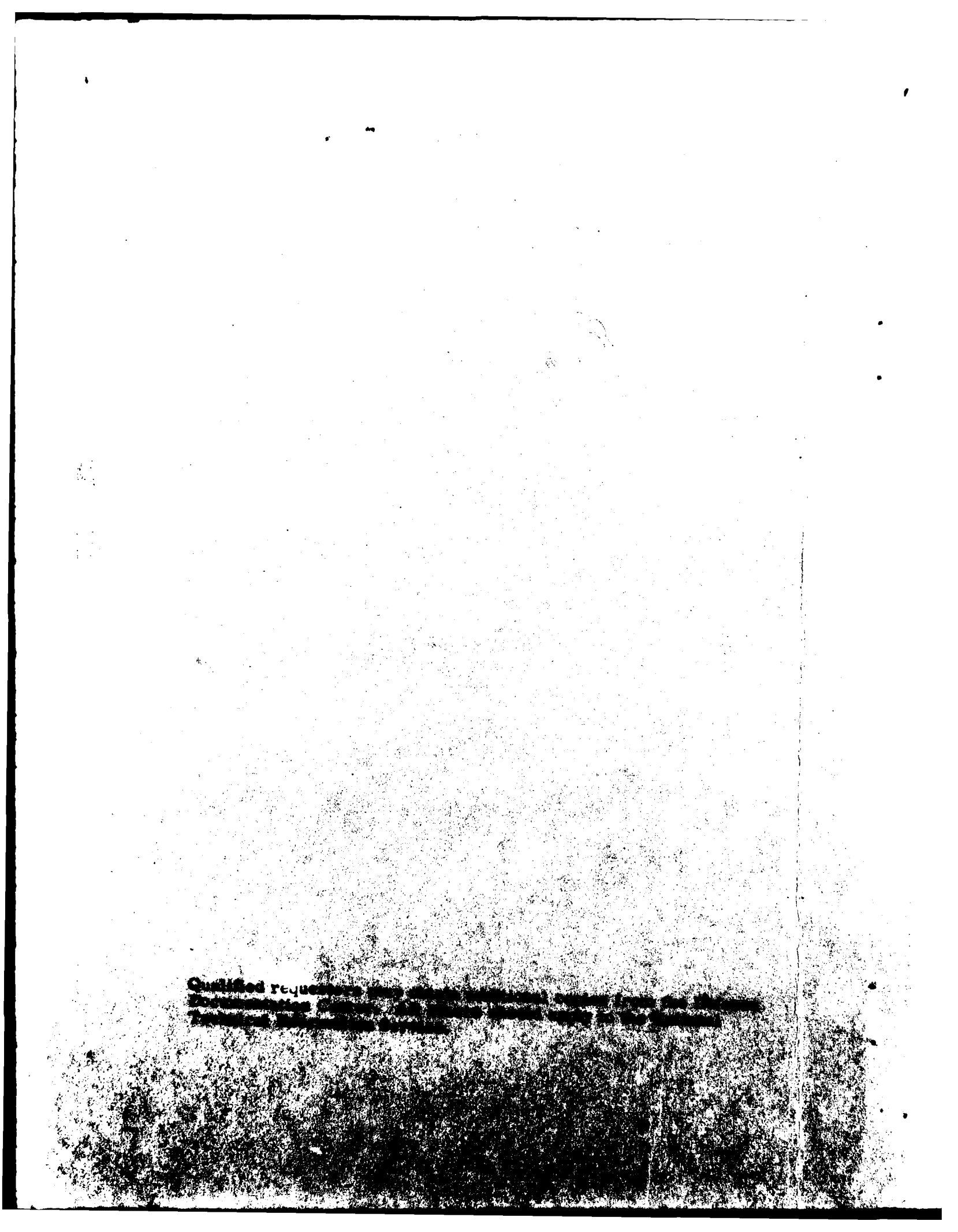

SECURITY CLASSIFICATION OF THIS PAGE (When Data Entered)

REPORT DOCUMENTATION PAGE

READ INSTRUCTIONS BEFORE COMPLETING FORM

1. REPORT NUMBER: AFGL-TR-79-0043	2. GOVT ACCESSION NO.: AD-A082579
3. RECIPIENT'S CATALOG NUMBER: VI-465	
4. TITLE (and Subtitle): EVALUATION AND DEVELOPMENT OF ADVANCED HIGH ALTITUDE EXPERIMENTS AND SYSTEMS	5. TYPE OF REPORT & PERIOD COVERED: FINAL REPORT, 15 May 76 - 1 Dec 78
	6. PERFORMING ORG. REPORT NUMBER
7. AUTHOR(s): J. W. Carpenter, W.P. Reidy, T. Zehnpfennig, C. Humphrey, O. Shepherd, A. Hurd, H.J.P. Smith	8. CONTRACT OR GRANT NUMBER(s): F-19628-76-C-0198
9. PERFORMING ORGANIZATION NAME AND ADDRESS: Visidyne, Inc., 19 Third Avenue, Northwest Industrial Park, Burlington, Massachusetts	10. PROGRAM ELEMENT, PROJECT, TASK AREA & WORK UNIT NUMBERS: 61102F, 2310G4AD
11. CONTROLLING OFFICE NAME AND ADDRESS: Air Force Geophysics Laboratory, Hanscom AFB, Massachusetts 01731, Monitor: Mr. John A. Sandock/OPR/1	12. REPORT DATE: 1 Dec 1978
	13. NUMBER OF PAGES: 88
14. MONITORING AGENCY NAME & ADDRESS (If different from Controlling Office)	15. SECURITY CLASS. (of this report): Unclassified
	15a. DECLASSIFICATION/DOWNGRADING SCHEDULE

16. DISTRIBUTION STATEMENT (of this Report)

Approved for pubic release; distribution unlimited

17. DISTRIBUTION STATEMENT (of the abstract entered in Block 20, if different from Report)

18. SUPPLEMENTARY NOTES

This work was sponsored in part by the Defense Nuclear Agency and the Space and Missile Systems Organization (SAMSO), and the contract work was conducted under the technical cognizance of Air Force Geophysics Laboratory (AFGL), AFSC.

19. KEY WORDS (Continue on reverse side if necessary and identify by block number)

High Altitude, Nuclear Effects Simulation, Energy Deposition Systems, Optical and IR Emission Codes, Rocketborne UV, and Visible Spectrometer, Auroral Electron Measurements.

20. ABSTRACT (Continue on reverse side if necessary and identify by block number)

This report covers development of advanced HAES experiments and related optical codes, development of rocketborne UV and visible spectrometers and particle analyzers, and evaluation and testing of Advanced Energy Deposition Systems (AEDS).

DD FORM 1 JAN 73 1473 EDITION OF 1 NOV 65 IS OBSOLETE

SECURITY CLASSIFICATION OF THIS PAGE (When Data Entered)

390562

TABLE OF CONTENTS

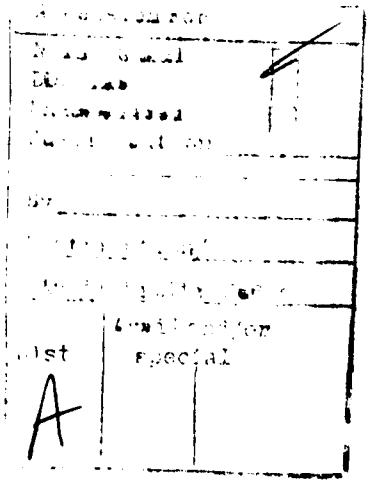

LIST OF ILLUSTRATIONS

LIST OF ILLUSTRATIONS (CONT.)

1.0 INTRODUCTION

This document is the final report on Contract F19628-76-C-0198. The effort on this contract discussed herein has been directed to the following:

1. Development of advanced High Altitude Effect Simulation (HAES) experiments to provide data necessary for the development of advanced optical codes (Section 2.0).

2. Development of a UV-visible spectrometer (Section 3.0) and particle analyzer instrumentation (Section 4.0).

3. Evaluation of techniques for Advanced Energy Deposition Systems (AEDS) and laboratory testing of the most promising techniques (Section 5.0).

Additional effort on this contract is described in another document which has a limited distribution[1]. This document covers the following:

1. Development of a Balloon Altitude Mosaic Measurements (BAMM) system and its associated mobile control system[2].

2. Laboratory studies of IR background suppression[3].

2.0 ADVANCED EXPERIMENTS FOR CODE DEVELOPMENT

In compliance with the requirements to provide inputs that enable better High Altitude Experimental Simulation (HAES) efforts to be performed, a study was conducted and programs developed and submitted to SAMSO, Aerospace, IBM Federal System, Westlake, CA. and Aerojet Electronic Systems Company, Azusa, CA. These efforts were limited in distribution to the aforementioned groups.

An analysis of test flight data was performed by R. Huppi (USU) and J. Reed (Visidyne) and reported in a common document issued from the Stewart Radiance Laboratory[4].

In conjunction with the development of the ROSCOE infrared code, the following models were provided to the Defense Nuclear Agency:

a. Aerosol Model
This model provides the absorption and scattering coefficients, as well as the augular scattering distribution, due to the aerosols as functions of altitude and type of atmosphere.

b. Wilson Cloud Model
If the humidity is sufficiently high, following a nuclear detonation near sea level, the rarefaction behind the strong shock wave causes the water vapor to condense to form a transitory cloud of complex shape and temporal history. This model provides the calculation, for arbitrary yield, altitude, and meteorological conditions, of the dimensions of the Wilson Cloud, if formed, and determines the log normal distribution of the water droplets at specified points within the cloud. These quantities are used to evaluate the transmission and scattering due to the Wilson Cloud.

c. Thermal Pulse Model
To account for the photon driven processes in the environs of a low or intermediate altitude fireball, a description has been provided of the ultraviolet output of the fireball as a function of yield, altitude of detonation, and time after detonation. The scaling thus derived is compared to available field data.

d. Strong Shock Model

For detonations in the altitude region from about 50 to 150 kilometers, the strong shock can provide a strong, moving source of short wavelength infrared. This model permits the shock history to be described along any arbitrary angle of intercept of the line of sight from the detector through the shock wave and the shock-driven chemistry, and the resulting chemiluminescence to be estimated.

e. Beta Patch Structure Model

Based on photographs taken in the field, the power spectral density of the structure in the beta patch has been determined and a model provided to permit its extrapolation to any exo-atmospheric detonations. This model allows evaluations of chosen system designs when operating against such an environment.

f. Plume Target Model

For comparison with the nuclear induced infrared backgrounds, generic solid and liquid fuel plume target models have been made for the short wavelength infrared emission as a function of time, altitude, and rocket stage number.

3.0 UV-VISIBLE SPECTROMETER SYSTEM

3.1 Instrument Description

The UV and Visible Spectrometers consist of two Ebert-Fastie scanning spectrometers. The individual specifications for each are listed in Tables 3.1 and 3.2.

The spectrometer design is shown schematically in Figure 3.1. An optical baffle is located in front of the spectrometer entrance slit to minimize the contribution of off-axis sources. This optical baffle is mounted on the spectrometer fore-optics assembly. The fore-optics assembly contains the mounting for the instrument window (fused silica for the visible spectrometer and MgF_2 for the UV spectrometer). The function of the window is to provide a hermetic sealed optical path between the spectrometers and the payload class 200 clean area common to all of the instrument entrance apertures. Also incorporated in the fore-optics section is the alternate scan attenuator disc and its driver mechanism. The function of the alternate scan attenuator is to increase the dynamic range of each spectrometer by a factor of 100. The disc consists of a clear substrate having a neutral density 2.0 (typ.) coating over one-half (180^{o}) of its transmission area. With the disc located before the spectrometer entrance slit and rotated once for every two grating scans, a normal spectrum is obtained followed by a spectrum attenuator by a factor of 100. The mechanical drive of the alternate scan attenuator is obtained directly from the grating drive by means of a timing belt. The predicted radiances of the various emissions to be measured in the EXCEDE experiment vary by orders of magnitude. However, the alternate scan attenuator disc permits measurement of both weak and strong spectral emissions (see spectrometer calibration data). The measured transmission of the alternate scan attenuator is shown in Figures 3.2 and 3.3.

Figure 3.4 is a block diagram of the instrument electronics and Table 3.3 specifies the data format. The geometry of the experiment is shown in Figures 3.5 and 3.6.

TABLE 3.1

VISIBLE SPECTROMETER SPECIFICATIONS

TYPE:	Ebert-Fastie Scanning Spectrometer
FOCAL LENGTH:	1/4 Meter
WAVELENGTH RANGE:	3800Å to 8000Å
SPECTRAL RESOLUTION:	12.8Å
SLIT WIDTH:	0.0443 cm
SLIT LENGTH:	3.40 cm
SLIT AREA:	0.151 cm^2
FIELD OF VIEW:	12^o x 12^o
$A\Omega$:	7×10^{-3} cm^2-sr
GRATING:	1200 ℓ/mm, Blazed at 5000Å Al and SiO_2 Coatings
SPECTRAL SCAN PERIOD:	3.80 Seconds
DATA SAMPLING RATE:	400 Samples/Second
MAXIMUM COUNT RATE:	1.64×10^4 Counts/Sample 6.55×10^6 Counts/Second

TABLE 3.2

UV SPECTROMETER SPECIFICATIONS

TYPE:	Ebert-Fastie Scanning Spectrometer
FOCAL LENGTH:	1/4 Meter
WAVELENGTH:	1500Å to 3000Å
SPECTRAL RESOLUTION:	8.6Å
SLIT WIDTH:	0.0517 cm
SLIT LENGTH:	3.40 cm
SLIT AREA:	0.176 cm^2
FIELD OF VIEW:	12^o x 12^o
AΩ:	8×10^{-3} cm^2-sr
GRATING:	2400 ℓ/mm. Blazed at 3000Å Al and MgF_2 Coatings
SPECTRAL SCAN PERIOD:	1.90 Seconds
DATA SAMPLING RATE:	400 Samples/Sec
MAXIMUM COUNT RATE:	1.64×10^4 Counts/Sample 6.55×10^6 Counts/Second

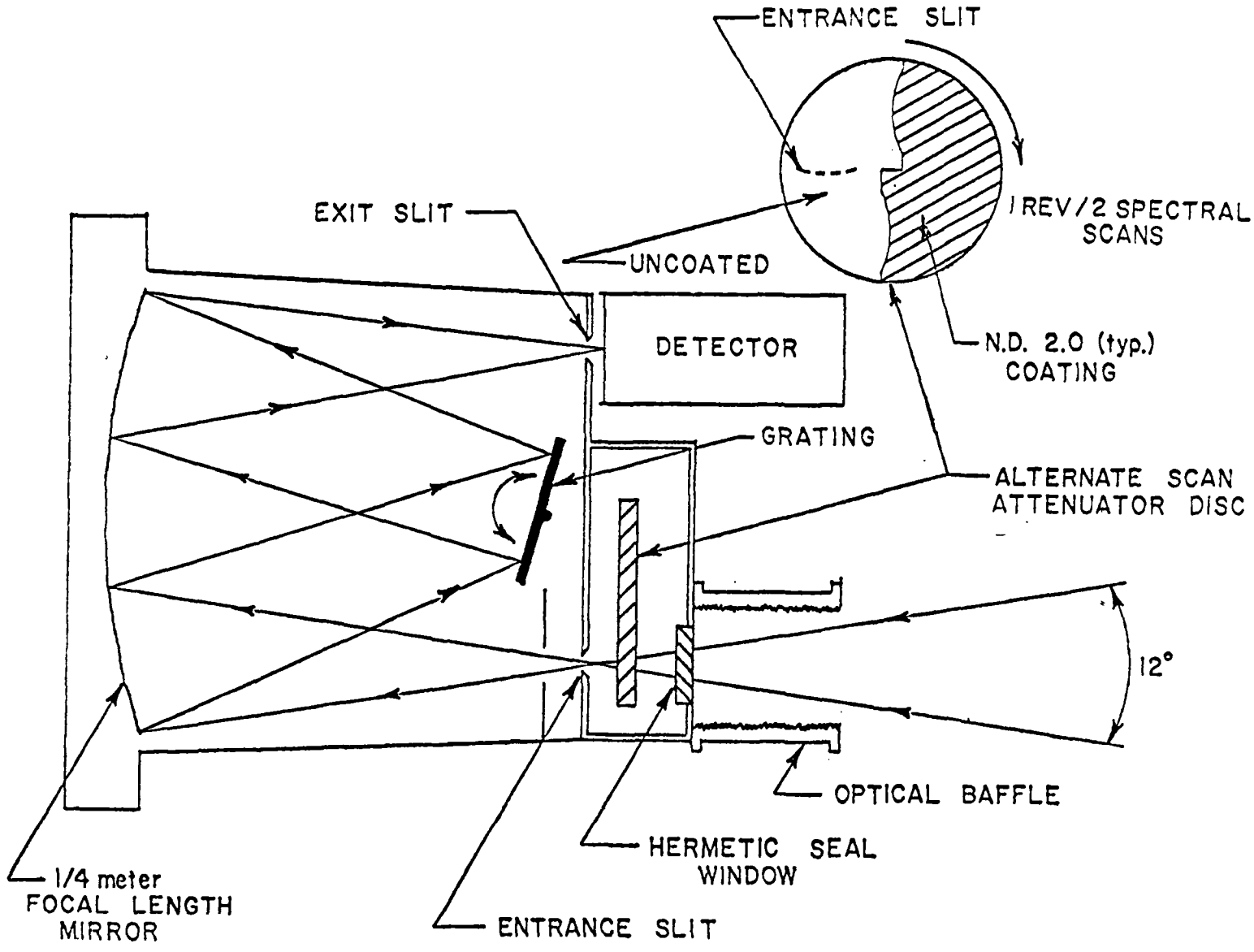

FIGURE 3.1 SPECTROMETER OPTICAL SCHEMATIC

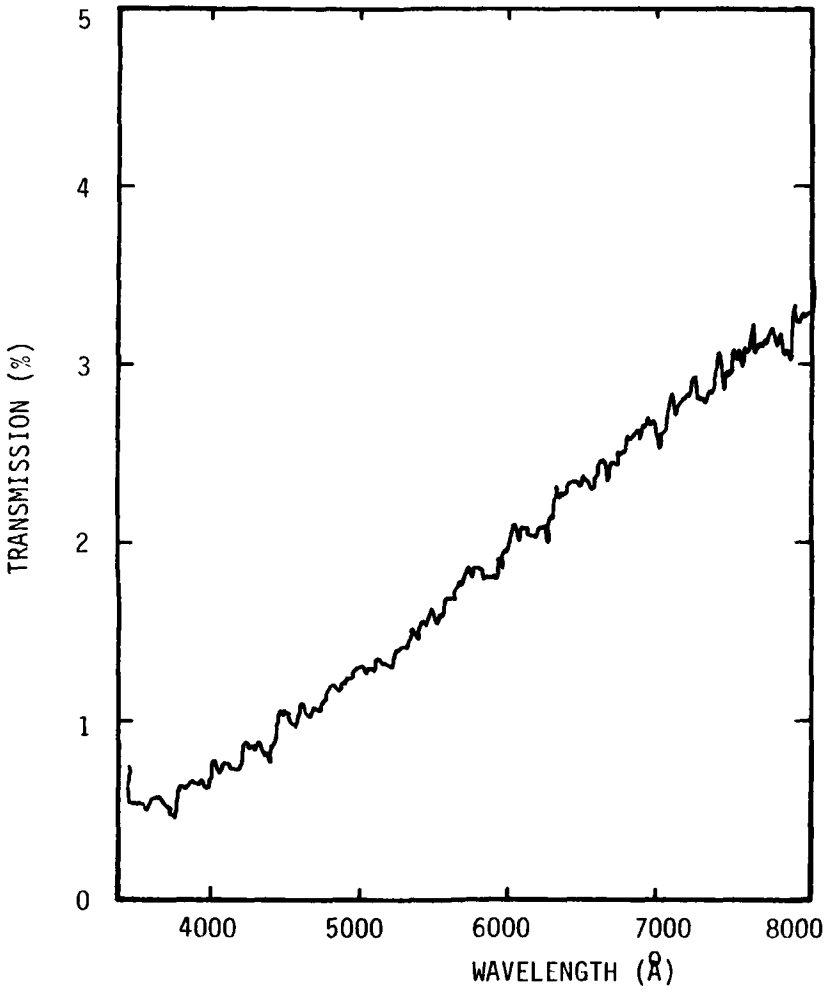

FIGURE 3.2 VISIBLE SPECTROMETER, SPECTRAL TRANSMISSION, ALTERNATE SCAN ATTENUATOR

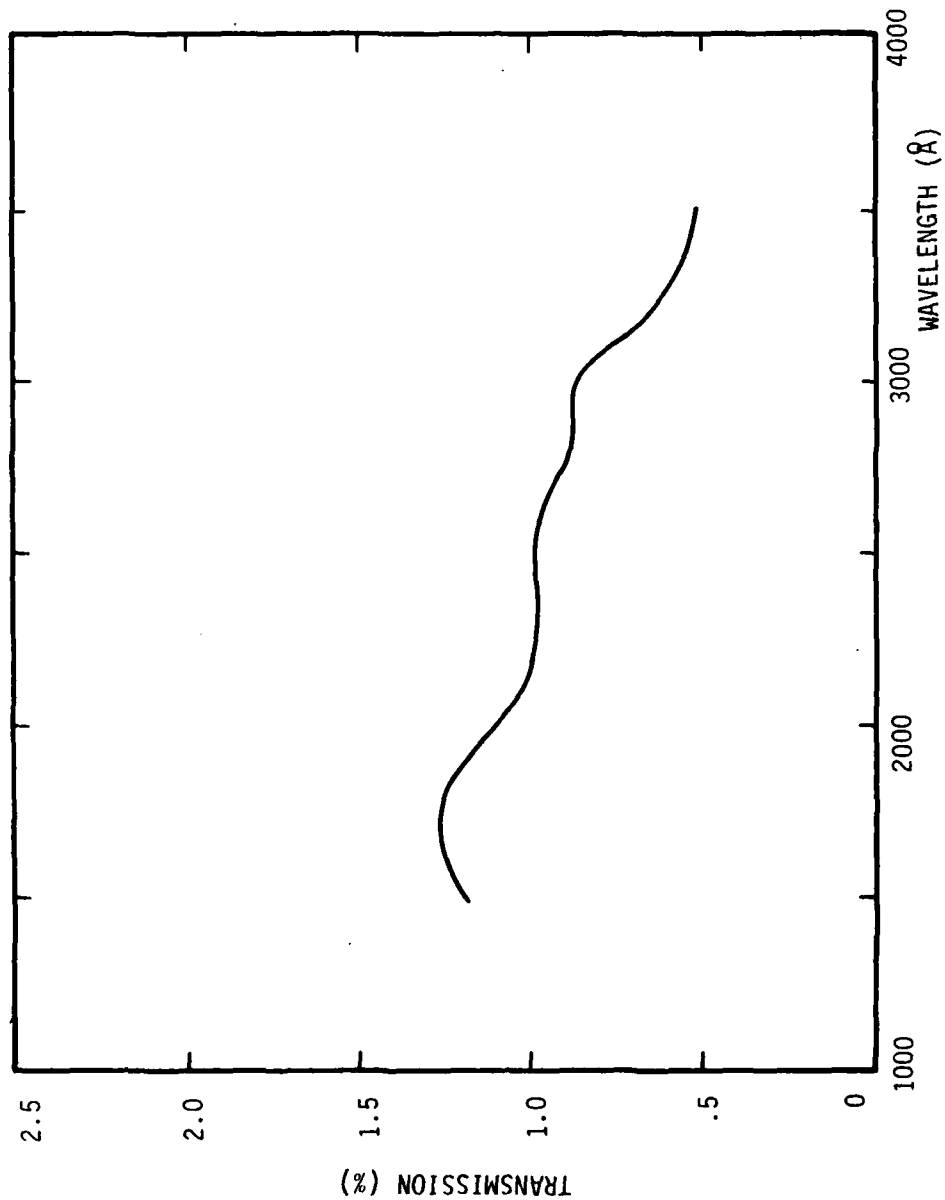

FIGURE 3.3 UV SPECTROMETER, SPECTRAL TRANSMISSION, ALTERNATE SCAN ATTENUATOR

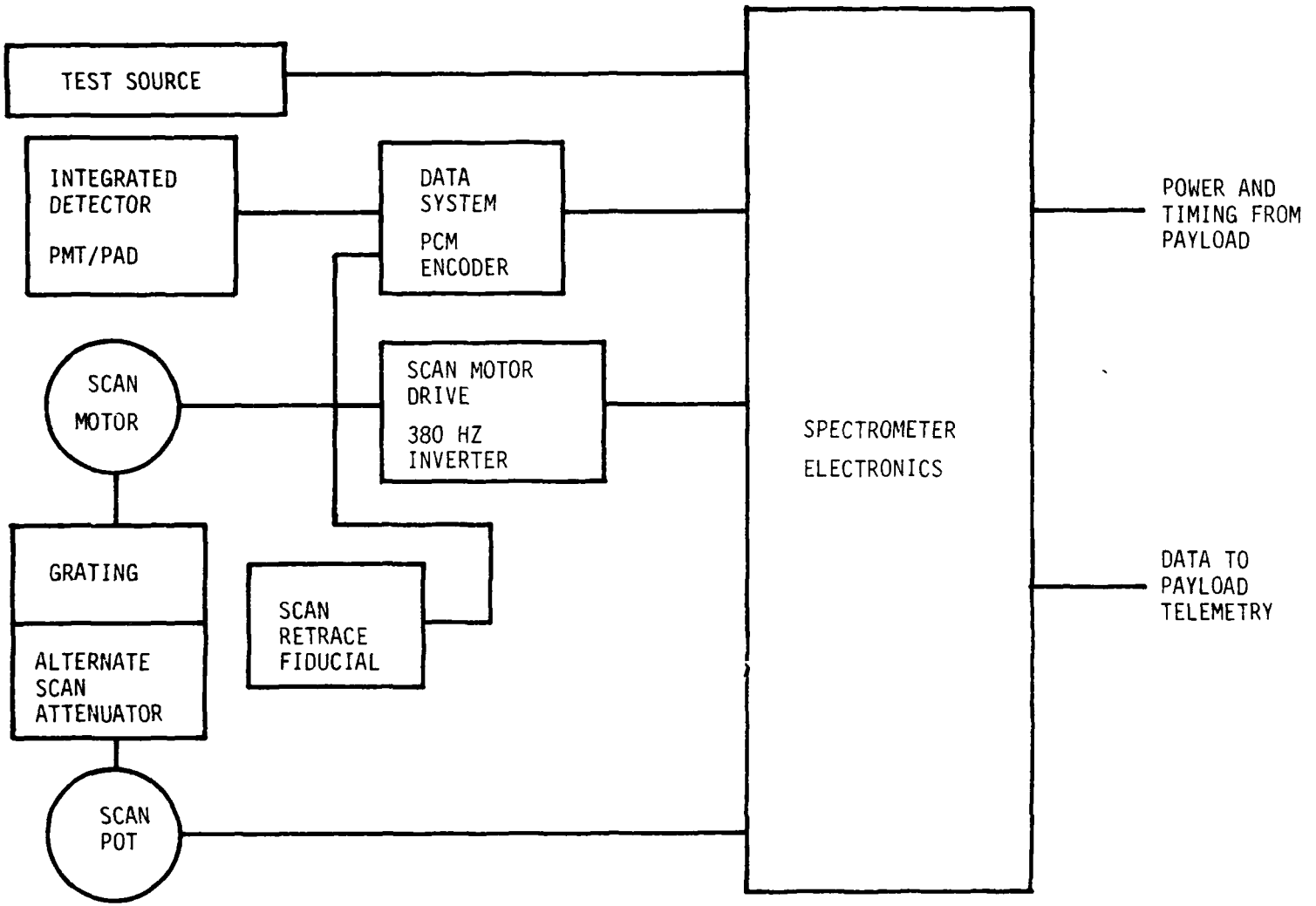

FIGURE 3.4 SPECTROMETER ELECTRONICS BLOCK DIAGRAM

TABLE 3.3

UV AND VISIBLE SPECTROMETER SPECIFICATION DATA FORMAT

DATA FORMAT:	Pulse Count Pulse Code Modulation (PCM)
SCAN SYNC:	2.5 Volt Pulse, 156 μsec Wide, Bit 15
WORD SYNC:	5 Volt Pulse, 156 μsec Wide, Bit 16
WORD LENGTH:	14 Bits Count Data Plus 1 Bit Word Sync Plus 1 Bit Scan Sync
WORD FORMAT:	NRZ-L 1 - 2.5 Volts 0 - 0.0 Volts
MAXIMUM DATA RATE:	6.4 K Bits/Sec
SAMPLING RATE:	400 Samples/Sec
SAMPLING TIME:	2.5 msec

	UV SPECTROMETER	VISIBLE SPECTROMETER
SCAN TIME:	1.90 Sec	3.80 Sec
DATA TIME:	1.82 Sec	3.64 Sec
RETRACE TIME:	0.08 Sec	0.16 Sec
SPECTRAL SCAN RATE:	824 Å/Sec	1100 Å/Sec
OVERSAMPLING FACTOR:	~4	~4
RESOLUTION:	8 Å	12.8 Å
Å/SAMPLE:	2.1	2.9

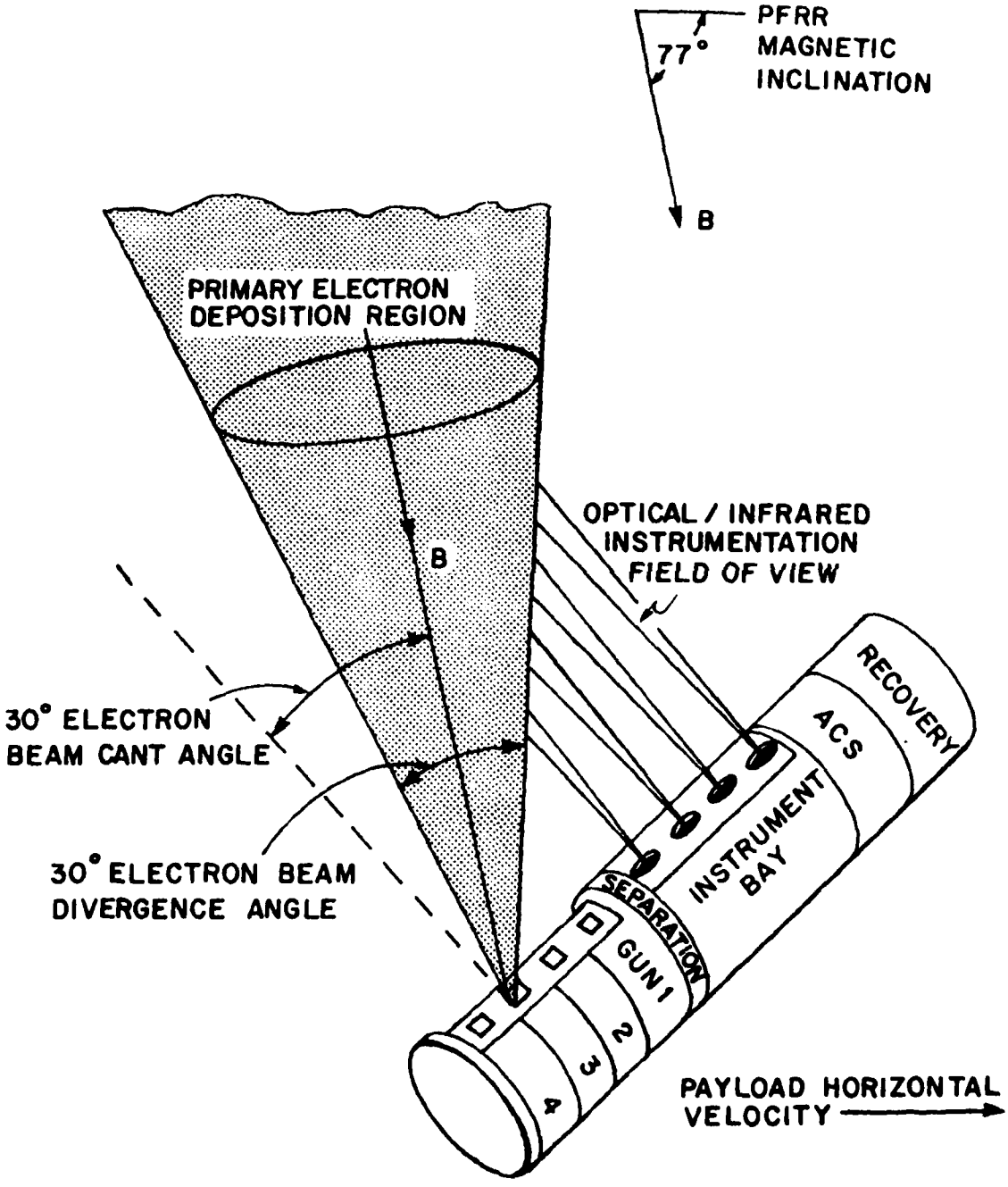

FIGURE 3.5 PAYLOAD ORIENTATION FOR EXCEDE II

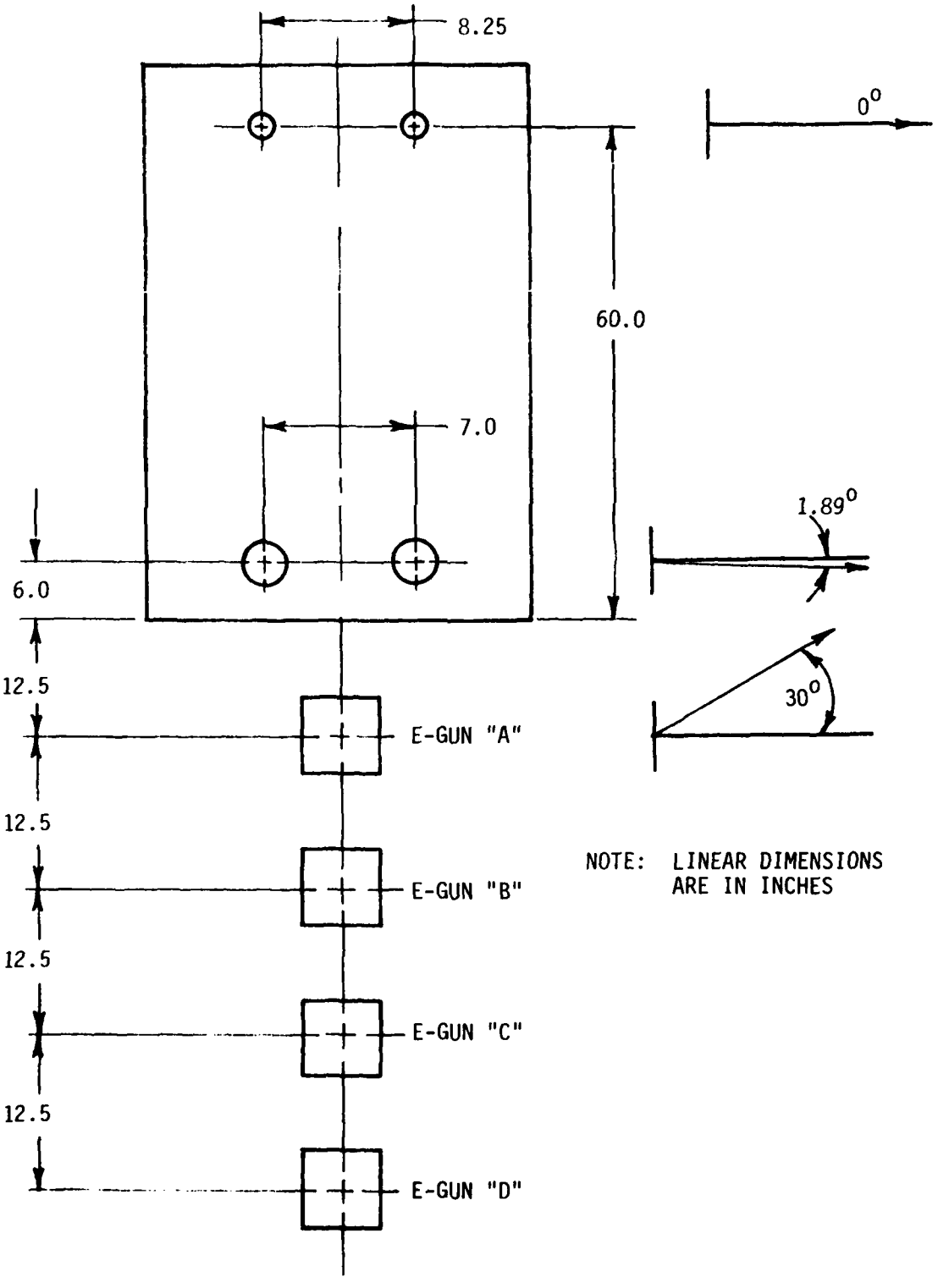

FIGURE 3.6 EXCEDE PAYLOAD SYSTEM GEOMETRY

3.2 Instrument Calibration

3.2.1 Spectral Calibration

On 7 July 1978, the UV and Visible Spectrometers were taken to AFGL for absolute calibration. The experimental setup is shown schematically in Figure 3.7 and the relationship between source brightness and photons entering the spectrometers is given in Table 3.4. The calibration procedure is summarized in the following paragraphs.

The absolute radiation source for this calibration was an Aerojet high temperature blackbody operated at 2440^{o}C (typ.). Radiation intensity was controlled by a variable aperture plate. A spatially extended source of blackbody radiation was obtained by using a screen painted with Kodak white reflectance paint and positioned 1.2 meters from the blackbody aperture. The spectrometers viewed the radiated screen such that both the spectrometers' field and aperture were filled. A slow scan capability was added to each spectrometer by coupling a low rpm dc motor onto the grating drive. This permitted operation at approximately 30 seconds/scan. The pulses out of the spectrometer pulse amplitude discriminator were integrated and the resulting analog signal used to drive the X axis of an X-Y recorder. The Y axis of the recorder was driven by the wavelength monitor potentiometer on the spectrometer grating drive.

With the spectrometer viewing the radiated screen, spectra covering the range of 4000Å to 8000Å were run with various apertures and glass filters. X-Y plots of these spectra were recorded on graph paper. Figure 3.8 is a typical example. The spectrometer PCM binary count data were correlated with recorded analog voltage to obtain a calibration constant (counts/sec/volt). The spectrometer wavelength span was calibrated by recording the spectra obtained when viewing an Oriel xenon lamp. The above data in a PCM format was recorded on analog tape using a CP-100 tape recorder. For this data, the flight scan mode was used (3.8 sec/scan). From these tests, the absolute spectral response of the Visible Spectrometer was defined. By the use of short wavelength blocking filters, the absence of a scattered light problem in the spectrometer was confirmed.

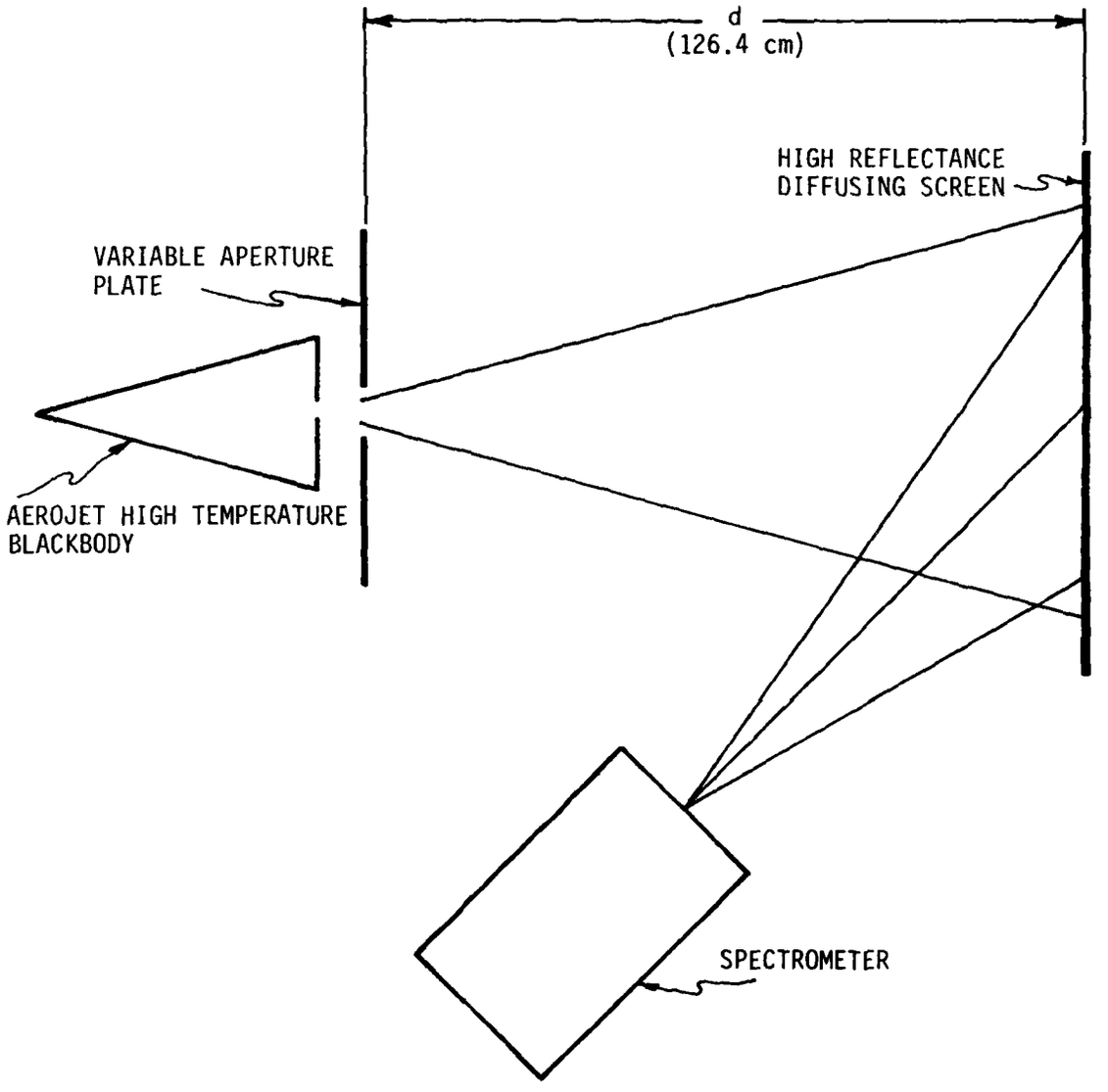

FIGURE 3.7 SPECTROMETER ABSOLUTE CALIBRATION GEOMETRY

TABLE 3.4
CALIBRATION SOURCE STRENGTH

$$N \text{ (Photons/Sec)} = \frac{W(\lambda)\ \Delta\lambda\ \frac{\lambda}{hc}}{\pi} \quad \frac{A_s}{d^2} \quad \frac{A\Omega}{\pi}$$

WHERE:

N	=	Photons/sec incident on the entrance aperture of the instrument being calibrated
$W(\lambda)$	=	Blackbody radiance (watts/cm^2-μm) at wavelength λ
$\Delta\lambda$	=	Spectral resolution (μm) of the spectrometer
$\frac{\lambda}{hc}$	=	Photons/joule at wavelength λ
A_s	=	Blackbody aperture area (cm^2)
d	=	Distance from blackbody aperture to screen (cm)
A	=	Spectrometer entrance slit area (cm^2)
Ω	=	Spectrometer solid angle (sr)

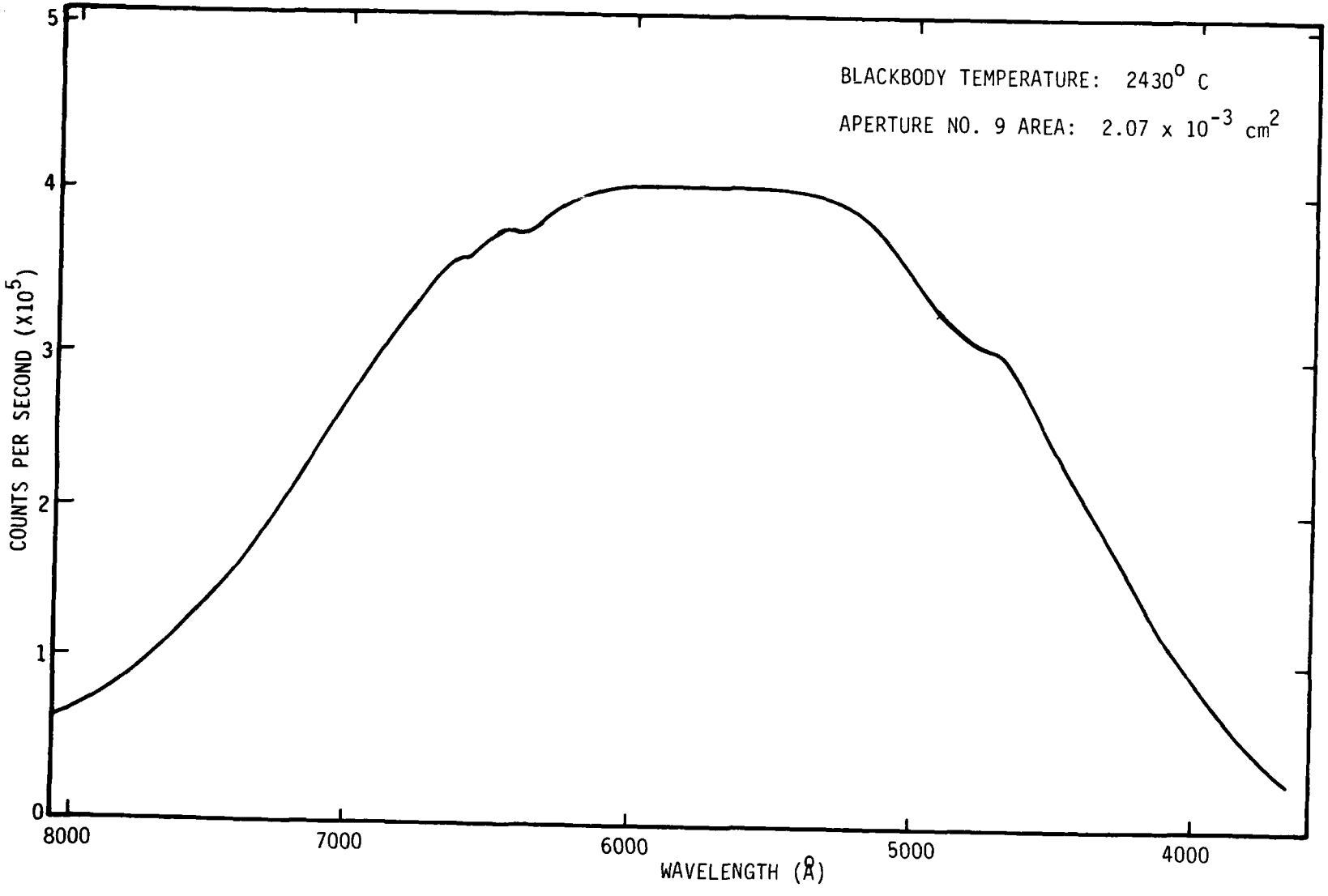

FIGURE 3.8 VISIBLE SPECTROMETER, FULL FIELD CALIBRATION, BLACKBODY SOURCE

The UV Spectrometer was set up in a similar manner and the above tests repeated for the 2000Å to 3000Å spectral range. A relative radiation source, a hydrogen lamp, was viewed to obtain the relative spectral response between 3000Å and 2000Å. The absolute response of 3000Å was obtained from blackbody data. Figures 3.9 and 3.10 are typical examples. From these tests, the absolute spectral response of the UV Spectrometer was obtained.

3.2.2 Spectrometer Field of View Calibration

The UV and Visible Spectrometers were subjected to full field mapping as part of the instrument calibration.

The spectrometer to be calibrated was mounted on a two axis gimbal mount. One axis (elevation) of the gimbal was coupled to a potentiometer. Both axes were manually adjustable.

A tungsten halogen lamp was used as a point source radiator.

The spectrometer was scanned in elevation with respect to the point source. The elevation potentiometer generated an angle voltage which was fed to the Y input of and X-Y plotter. The X axis was inputted with a voltage proportional to the integrated pulse count rate out of the spectrometer.

Elevation scans were run, typically, for every 0.5 degrees of azimuth. This mesh was decreased at the field edges so as to more highly resolve the instrument field cut-off function. Figure 3.11 is a typical example.

3.2.3 Calibration Results

Using the data generated in the calibration discussed above, we have calculated the spectrometer efficiency (ε) as a function of wavelength.

$$\varepsilon \equiv \frac{n\ (\text{count/sec})}{n\ (\text{photon/sec})} \equiv \frac{n'\ (\text{count/sample})}{n'\ (\text{photon/sample})}$$

where: $400\ n' = n$

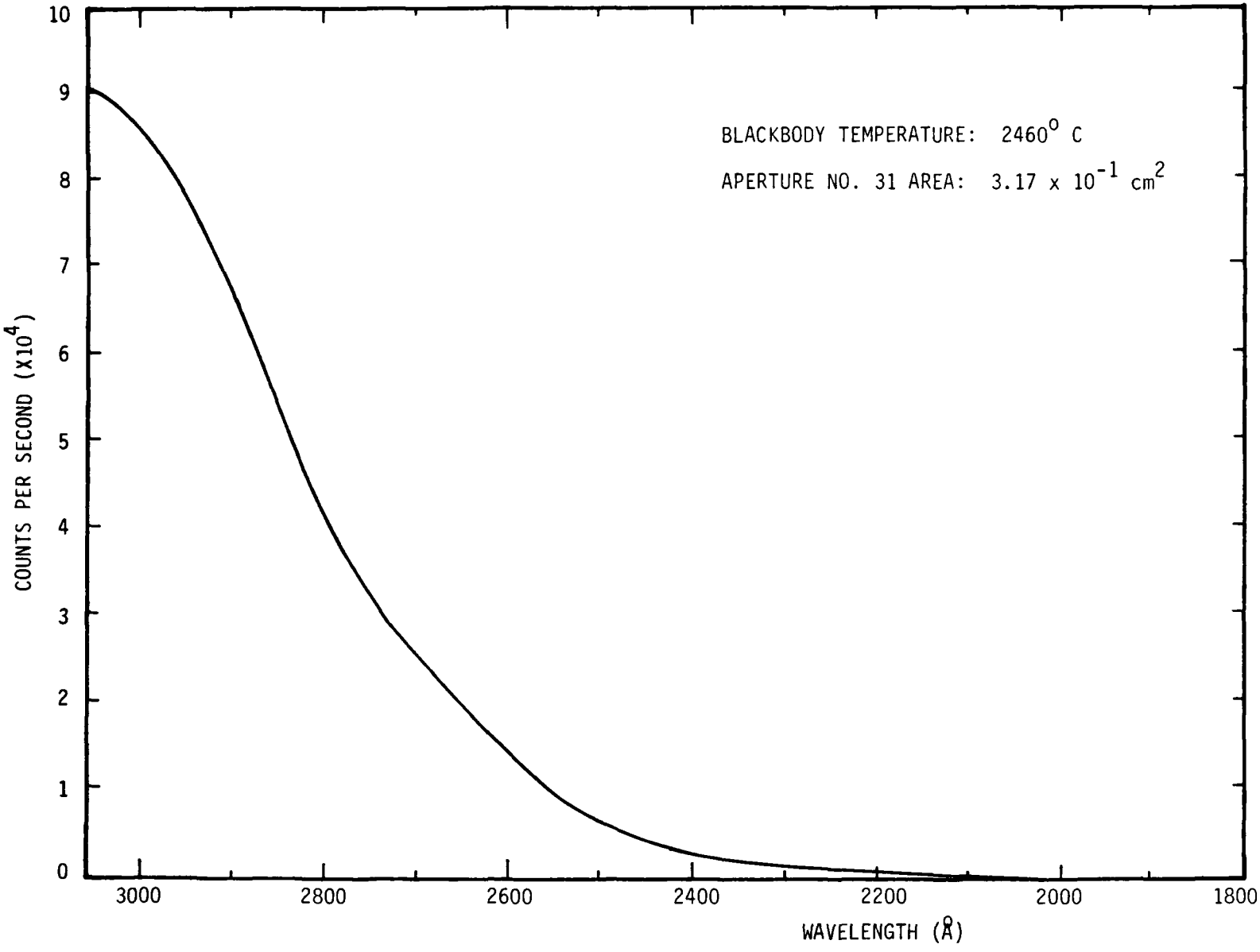

FIGURE 3.9 UV SPECTROMETER, FULL FIELD CALIBRATION, BLACKBODY SOURCE

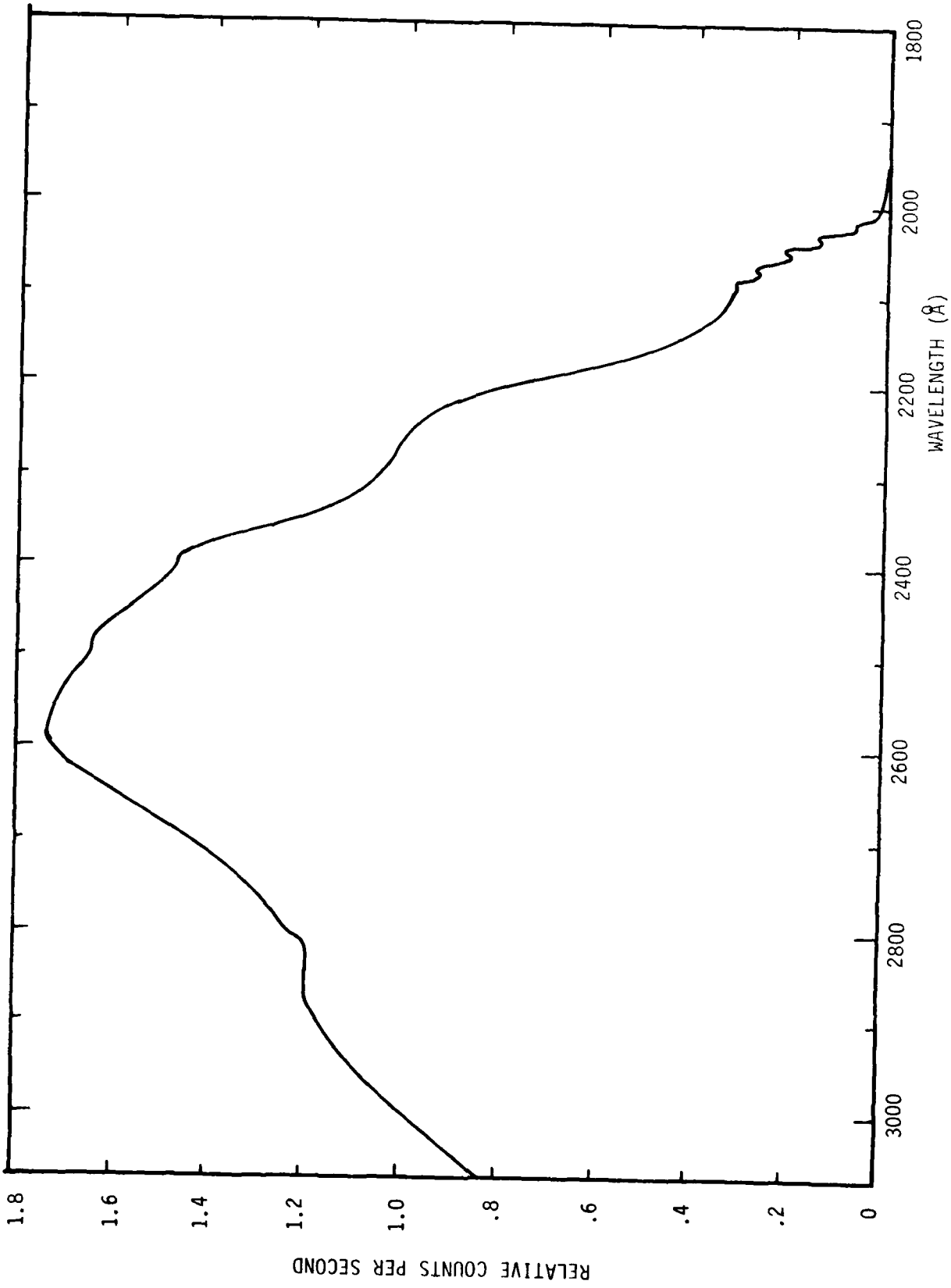

FIGURE 3.10 UV SPECTROMETER, FULL FIELD CALIBRATION, HYDROGEN LAMP SOURCE

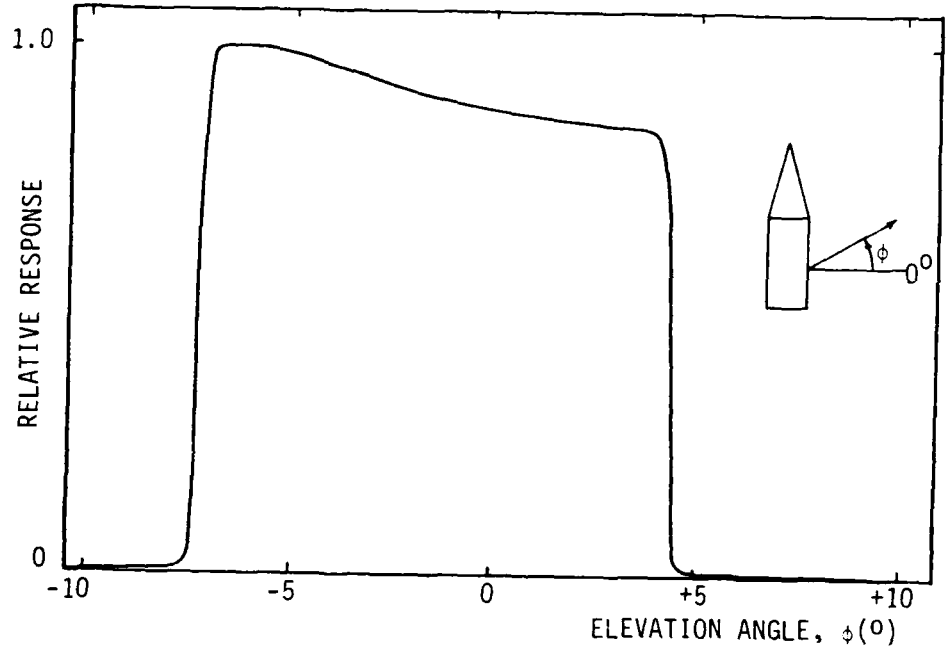

FIGURE 3.11 UV SPECTROMETER, RELATIVE RESPONSE VS. ELEVATION ANGLE

Table 3.5 lists the relevant parameters for the Visible Spectrometer calibration and Table 3.6 lists the calibration results. Tables 3.7 and 3.8 provide similar information for the UV Spectrometer.

We have also calculated the following quantities for specific line emissions:

MRMAX	Predicted radiance (megarayleighs) at 90 km altitude and 120 kw E-gun emission.
MRMIN	Predicted radiance (megarayleighs) at 130 km altitude and 30 kw E-gun emission.
MR	Predicted radiance (megarayleighs) at 110 km altitude and 120 kw E-gun emission.
MRSAT	Radiance (megarayleighs) at which the spectrometer data system overflows. Upper limit of valid data for a non-attenuated spectral scan.
MRSAT2	Radiance (megarayleighs) at which spectrometer data system overflows. Upper limit of valid data for an attenuated spectral scan.
MR.05	Maximum radiance (megarayleighs) required for data having a 5 percent statistical error.
MR.1	Maximum radiance (megarayleighs) required for data having a 10 percent statistical error.

These are tabulated in Tables 3.9 and 3.10 for the visible and UV spectrometers respectively.

3.3 UV DIODES

The function of the UV diodes was to measure the wide band UV irradiance in the 1250Å to 3000Å spectral interval. Diode specifications are given in Table 3.11.

The UV-1 diode is shown in Figure 3.12. It employs as a detector an ITT Model F4115 biplanar photodiode having a solar blind cesium

TABLE 3.5

EXCEDE VISIBLE SPECTROMETER PARAMETERS

SPECTRAL RESOLUTION:	12.8 Angstroms
SLIT LENGTH:	3.40 cm
SLIT WIDTH:	.0443 cm
AREA	1.51E-01 cm^2
FIELD OF VIEW:	12.0 degrees x 12.0 degrees
SOLID ANGLE:	4.42E-02 sr
ETENDUE:	6.66E-03 cm^2-sr
SPECTRAL SCAN TIME:	3.80 seconds
INTEGRATION TIME:	2.5 milliseconds
BLACKBODY TEMPERATURE:	2430^o C
APERTURE AREA:	2.07E-03 cm^2
SCREEN DISTANCE:	126.1 cm

TABLE 3.6

EXCEDE VISIBLE SPECTROMETER CALIBRATION RESULTS

WAVELENGTH (ANGSTROMS)	LINE WIDTH	BLACK BODY RADIANCE (WATTS/CM**2/ MICROMETER)	CAL (PHOTONS /SEC)	CAL (COUNT /SEC)	NEUTRAL DENSITY FILTER TRANSMISSION	E SPECTROMETER EFFICIENCY	K (MR/COUNT /SEC)	KPRIME (MR/COUNT /BIN)
3314.	1.	5.05E+00	1.12E+06	8.47E+04	6.50E-03	.076	2.50E-08	9.98E-06
4059.	1.	5.85E+00	1.57E+06	1.11E+05	7.00E-03	.071	2.68E-08	1.07E-05
4278.	1.	1.03E+01	2.49E+06	1.75E+05	8.10E-03	.070	2.59E-08	1.03E-05
4709.	1.	1.99E+01	5.31E+06	3.10E+05	1.03E-02	.058	3.23E-08	1.29E-05
5228.	1.	3.63E+01	1.07E+07	3.94E+05	1.40E-02	.037	5.14E-08	2.06E-05
5577.	1.	4.97E+01	1.57E+07	4.15E+05	1.61E-02	.026	7.13E-08	2.86E-05
5609.	50.	5.10E+01	1.62E+07	4.15E+05	1.66E-02	.026	2.87E-07	1.15E-04
5900.	50.	6.75E+01	2.29E+07	4.12E+05	1.94E-02	.018	4.92E-07	1.97E-04
6545.	60.	9.15E+01	3.39E+07	3.60E+05	2.35E-02	.011	7.89E-07	3.16E-04
6624.	60.	9.50E+01	3.56E+07	3.56E+05	2.42E-02	.010	8.61E-07	3.44E-04
6705.	60.	9.85E+01	3.74E+07	3.58E+05	2.48E-02	.010	9.24E-07	3.69E-04
6769.	65.	1.02E+02	3.92E+07	3.24E+05	2.52E-02	.008	1.16E-06	4.64E-04
6785.	65.	1.02E+02	3.91E+07	2.89E+05	2.60E-02	.007	1.30E-06	5.19E-04
7387.	75.	1.26E+02	5.28E+07	1.90E+05	2.89E-02	.004	3.07E-06	1.23E-03
7505.	75.	1.31E+02	5.55E+07	1.43E+05	2.98E-02	.003	4.29E-06	1.72E-03
7627.	75.	1.35E+02	5.82E+07	1.20E+05	3.04E-02	.002	5.37E-06	2.15E-03
7724.	75.	1.38E+02	6.04E+07	1.08E+05	3.10E-02	.002	6.13E-06	2.43E-03
7854.	50.	1.43E+02	6.34E+07	8.03E+04	3.15E-02	.001	9.32E-06	3.73E-03

TABLE 3.7

EXCEDE ULTRAVIOLET SPECTROMETER PARAMETERS

SPECTRAL RESOLUTION:	8.6 Angstroms
SLIT LENGTH:	3.40 cm
SLIT WIDTH:	.0517 cm
AREA:	1.76E-01 cm^2
FIELD OF VIEW:	12.0 degrees x 12.0 degrees
SOLID ANGLE:	4.42E-02 sr
ETENDUE:	7.77E-03 cm^2-sr
SPECTRAL SCAN TIME:	1.90 seconds
INTEGRATION TIME:	2.5 milliseconds
BLACKBODY TEMPERATURE:	2460^o C
APERTURE AREA:	3.17E-01 cm^2
SCREEN DISTANCE:	126.1 cm

TABLE 3.8

EXCEDE ULTRAVIOLET SPECTROMETER CALIBRATION RESULTS

WAVELENGTH (ANGSTROMS)	LINE WIDTH	BLACK BODY RADIANCE (WATTS/CM**2/ MICROMETER)	CAL (PHOTONS /SEC)	CAL (COUNT /SEC)	NEUTRAL DENSITY FILTER TRANSMISSION	E SPECTROMETER EFFICIENCY	K (MR/COUNT /SEC)	KPRIME (MR/COUNT /BIN)
2425.	1.	1.12E-01	1.85E+06	1.31E+05	9.80E-03	.071	2.29E-08	9.16E-06
2447.	1.	1.06E-01	1.76E+06	1.33E+05	9.80E-03	.076	2.14E-08	8.55E-06
2468.	1.	1.04E-01	1.74E+06	1.37E+05	9.80E-03	.079	2.05E-08	8.19E-06
2474.	1.	1.03E-01	1.73E+06	1.41E+05	9.80E-03	.081	1.99E-08	7.95E-06
2497.	1.	1.01E-01	1.71E+06	1.42E+05	9.90E-03	.083	1.95E-08	7.81E-06
2511.	1.	9.88E-02	1.69E+06	1.44E+05	9.90E-03	.086	1.89E-08	7.57E-06
2534.	1.	9.77E-02	1.68E+06	1.45E+05	9.90E-03	.087	1.87E-08	7.48E-06
2561.	1.	9.40E-02	1.64E+06	1.48E+05	9.80E-03	.091	1.78E-08	7.14E-06
2604.	1.	8.93E-02	1.58E+06	1.48E+05	9.70E-03	.094	1.72E-08	6.90E-06
2631.	1.	8.62E-02	1.54E+06	1.43E+05	9.60E-03	.093	1.74E-08	6.96E-06
2667.	1.	8.20E-02	1.49E+06	1.35E+05	9.50E-03	.091	1.78E-08	7.13E-06
2711.	1.	7.72E-02	1.42E+06	1.21E+05	9.40E-03	.085	1.90E-08	7.62E-06
2734.	1.	7.51E-02	1.39E+06	1.19E+05	9.30E-03	.085	1.90E-08	7.60E-06
2761.	1.	7.09E-02	1.33E+06	1.12E+05	9.20E-03	.084	1.93E-08	7.71E-06
2767.	1.	7.04E-02	1.32E+06	1.08E+05	9.00E-03	.082	1.98E-08	7.91E-06
2814.	1.	6.62E-02	1.27E+06	1.02E+05	8.90E-03	.081	2.00E-08	7.99E-06
2818.	1.	6.57E-02	1.26E+06	1.02E+05	8.90E-03	.081	1.99E-08	7.95E-06
2820.	1.	6.57E-02	1.26E+06	1.02E+05	8.80E-03	.081	1.99E-08	7.95E-06
2877.	1.	6.04E-02	1.18E+06	1.11E+05	8.80E-03	.094	1.73E-08	6.91E-06
2887.	1.	5.94E-02	1.16E+06	1.01E+05	8.80E-03	.087	1.87E-08	7.48E-06
2936.	1.	5.62E-02	1.12E+06	9.58E+04	8.80E-03	.085	1.89E-08	7.57E-06
2938.	1.	5.56E-02	1.11E+06	9.58E+04	8.80E-03	.086	1.87E-08	7.50E-06
2950.	1.	5.52E-02	1.11E+06	8.58E+04	8.80E-03	.078	2.09E-08	8.35E-06
2953.	1.	5.46E-02	1.10E+06	8.58E+04	8.80E-03	.078	2.07E-08	8.26E-06
2962.	1.	5.41E-02	1.09E+06	8.50E+04	8.80E-03	.078	2.07E-08	8.29E-06
2977.	1.	5.36E-02	1.08E+06	8.41E+04	8.70E-03	.078	2.08E-08	8.34E-06
2988.	1.	5.25E-02	1.07E+06	8.33E+04	8.70E-03	.078	2.07E-08	8.28E-06

TABLE 3.9

EXCEDE VISIBLE LINE EMISSIONS

WAVELENGTH	MR (H=110 KM (120 KW)	MR(MAX) (H=90 KM) (120 KW)	MR(MIN) (H=120 KM) (20 KW)	MRSAT	MRSAT2	MR.05	MR.1
3914.	4.00E+01	1.44E+03	4.80E+00	1.64E-01	2.52E+01	3.99E-03	9.98E-04
4059.	2.00E+00	7.20E+01	2.40E-01	1.75E-01	2.51E+01	4.28E-03	1.07E-03
4278.	1.30E+01	4.68E+02	1.56E+00	1.76E-01	2.16E+01	4.31E-03	1.08E-03
4709.	3.00E+00	1.08E+02	3.60E-01	2.12E-01	2.06E+01	5.17E-03	1.29E-03
5228.	6.00E-01	2.16E+01	7.20E-02	3.37E-01	2.41E+01	8.23E-03	2.06E-03
5577.	2.00E+00	7.20E+01	2.40E-01	4.67E-01	2.90E+01	1.14E-02	2.85E-03
5609.	4.00E+00	1.44E+02	4.80E-01	1.86E+00	1.13E+02	4.60E-02	1.15E-02
6000.	2.00E+00	7.20E+01	2.40E-01	3.23E+00	1.66E+02	7.88E-02	1.97E-02
6545.	5.00E+00	1.80E+02	6.00E-01	5.17E+00	2.20E+02	1.26E-01	3.16E-02
6624.	8.00E+00	2.88E+02	9.60E-01	5.64E+00	2.33E+02	1.38E-01	3.44E-02
6705.	1.10E+01	3.96E+02	1.32E+00	6.05E+00	2.44E+02	1.48E-01	3.69E-02
6789.	1.10E+01	3.96E+02	1.32E+00	7.60E+00	3.02E+02	1.86E-01	4.64E-02
6785.	5.00E+00	1.80E+02	6.00E-01	8.91E+00	3.27E+02	2.08E-01	5.19E-02
7387.	1.50E+01	5.40E+02	1.80E+00	2.01E+01	6.97E+02	4.92E-01	1.23E-01
7505.	3.00E+01	1.08E+03	3.60E+00	2.81E+01	9.44E+02	6.87E-01	1.72E-01
7627.	3.70E+01	1.33E+03	4.44E+00	3.52E+01	1.16E+03	8.59E-01	2.15E-01
7724.	3.30E+01	1.19E+03	3.96E+00	4.06E+01	1.31E+03	9.91E-01	2.48E-01
7854.	4.00E+01	1.44E+03	4.80E+00	6.10E+01	1.94E+03	1.49E+00	3.73E-01

TABLE 3.10

EXCEDE ULTRAVIOLET LINE EMISSIONS

WAVELENGTH	MR (H=110 KM (120 KW)	MR(MAX) (H=90 KM (120 KW)	MR(MIN) (H=120 KM (30 KW)	MRSAT	MRSAT2	MR.05	MR.1
2425.	6.00E-02	2.16E+00	7.20E-03	1.50E-01	1.53E+01	3.67E-03	9.16E-04
2443.	4.00E-02	1.44E+00	4.80E-03	1.40E-01	1.43E+01	3.42E-03	8.55E-04
2462.	5.70E-01	2.05E+01	6.84E-02	1.34E-01	1.37E+01	3.28E-03	8.19E-04
2474.	1.20E-01	4.32E+01	1.44E-02	1.30E-01	1.33E+01	3.18E-03	7.95E-04
2493.	2.00E-02	7.20E-01	2.40E-03	1.26E-01	1.29E+01	3.12E-03	7.81E-04
2511.	1.80E-01	5.48E+00	2.16E-02	1.24E-01	1.25E+01	3.03E-03	7.57E-04
2524.	1.10E-01	3.96E+00	1.32E-02	1.23E-01	1.24E+01	2.99E-03	7.48E-04
2561.	3.70E-01	1.33E+01	4.44E-02	1.17E-01	1.19E+01	2.86E-03	7.14E-04
2604.	9.80E-01	3.53E+01	1.18E-01	1.13E-01	1.16E+01	2.76E-03	6.90E-04
2631.	3.00E-02	1.08E+00	3.60E-03	1.14E-01	1.19E+01	2.70E-03	6.96E-04
2667.	1.30E-01	4.68E+00	1.56E-02	1.17E-01	1.23E+01	2.85E-03	7.13E-04
2711.	4.60E-01	1.66E+01	5.52E-02	1.25E-01	1.33E+01	3.05E-03	7.62E-04
2724.	7.00E-02	2.52E+00	8.40E-03	1.25E-01	1.34E+01	3.04E-03	7.60E-04
2761.	1.23E+00	4.43E+01	1.48E-01	1.26E-01	1.37E+01	3.08E-03	7.71E-04
2767.	1.90E-01	6.84E+00	2.28E-02	1.30E-01	1.44E+01	3.16E-03	7.91E-04
2814.	1.00E-01	3.60E+00	1.20E-02	1.31E-01	1.47E+01	3.20E-03	7.99E-04
2816.	2.90E-01	1.04E+01	3.48E-02	1.30E-01	1.46E+01	3.18E-03	7.95E-04
2820.	5.00E-02	1.80E+00	6.00E-03	1.30E-01	1.48E+01	3.18E-03	7.95E-04
2877.	1.30E-01	4.68E+00	1.56E-02	1.13E-01	1.29E+01	2.76E-03	6.91E-04
2887.	1.30E-01	4.68E+00	1.56E-02	1.23E-01	1.39E+01	2.99E-03	7.48E-04
2936.	1.16E+00	4.18E+01	1.39E-01	1.24E-01	1.41E+01	3.03E-03	7.57E-04
2938.	4.00E-01	1.44E+01	4.80E-02	1.23E-01	1.40E+01	3.00E-03	7.50E-04
2950.	4.00E-02	1.44E+00	4.80E-03	1.37E-01	1.55E+01	3.34E-03	8.35E-04
2953.	5.50E-01	1.98E+01	6.60E-02	1.35E-01	1.54E+01	3.31E-03	8.26E-04
2962.	9.00E-01	3.24E+01	1.08E-01	1.36E-01	1.54E+01	3.32E-03	8.29E-04
2977.	1.00E+00	3.60E+01	1.20E-01	1.37E-01	1.57E+01	3.34E-03	8.34E-04
2988.	9.30E-01	3.35E+01	1.12E-01	1.36E-01	1.56E+01	3.31E-03	8.28E-04

TABLE 3.11
UV DIODE SPECIFICATIONS

	UV-1	UV-2
SPECTRAL RANGE	1250Å to 3000Å	2000Å to 3000Å
DETECTOR	Photodiode	Photodiode
	CsTe Photocathode	CsTe Photocathode
	MgF_2 Window	UV Glass Window
DATA MODE	Current - Log Amplified	
DYNAMIC RANGE	10^4	
AREA	0.36 cm^2	
SOLID ANGLE (Effective)	0.76 sr	
ETENDUE	2.64×10^{-1} cm^2 - sr	
SENSITIVITY	$\frac{I_S \text{ (Diode Current)}}{\text{MR (Megarayleighs)}} = (\text{Q.E.}) \left(\frac{A\Omega \ e \ 10^{12}}{4\pi}\right) = 3.70 \times 10^{-10}$ a/MR	

TO CONVERT DATA TELEMETRY VOLTAGE TO MEGARAYLEIGHS:

$$MR = \{10^{(VA + B)}\}_{-1-D} K$$

WHERE:

A = -0.5
B = 4.50
D(UV-1) = 0.0
D(UV-2) = 1.24
$K = 2.7 \times 10^{-3}$ MR/mv

$MRMAX = 2.7 \times 10^{1}$ MR
$MRMIN = 2.7 \times 10^{-3}$ MR

IF MR < 0
THEN MR = 0

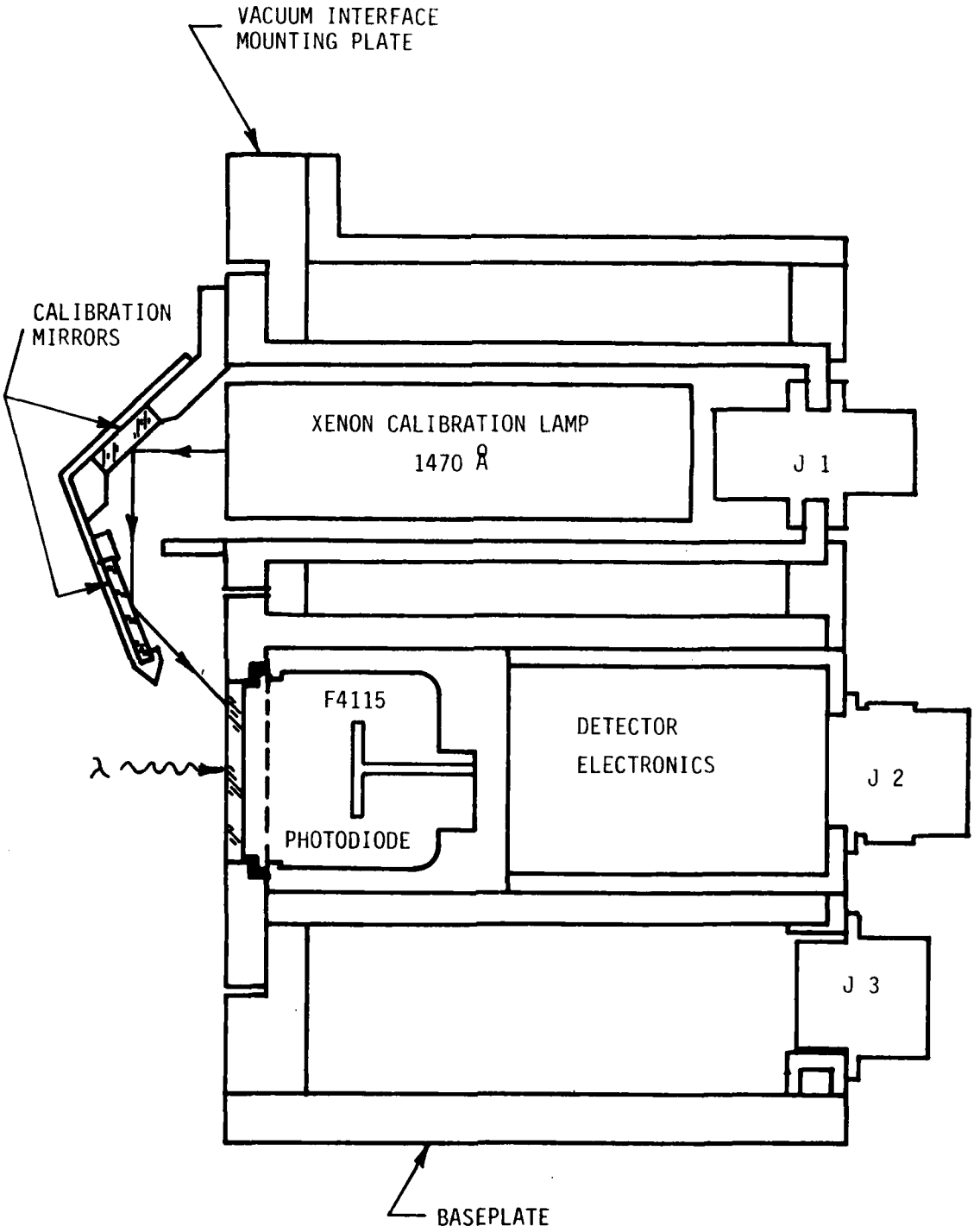

FIGURE 3.12 UV-1 DIODE

telluride photocathode. The photodetector is ideally suited for measuring large photocurrents. The output photocurrent is linear from 10^{-12} amps to 1 amp. The diode window is of UV quality magnesium fluoride secured to the tube envelope with a silver chloride seal. A high transmission mesh anode is located in front of the photocathode. MgF_2 was selected for the entrance window because it is more rugged and radiation-resistant and has a short wavelength cutoff below 1200Å. The detector does not require electron multiplication gain because of the anticipated high UV flux levels. Spectral response of the photodiode is shown in Figure 3.13. The spectral response of the biplanar photodiode was calibrated by the manufacturer, ITT.

The UV-2 photodiode is similar to the UV-1 except that the MgF_2 window is replaced by one of the UV transmitting glasses. Thus, the spectral range of UV-2 is from 2000Å to 3000Å.

Each UV photodiode is packaged integrally with its data log amplifier and power supply. The physical size is approximately 3 1/2 inches wide by 6 inches high by 6 inches deep and the weight is about one (1) pound. The maximum power required is 28 VDC, 100 ma.

Incorporated into the package is an EMR Model 582X-05 xenon 1470Å calibration source to enable in-flight diode calibration. The source has a sapphire window and emits more than 90% of its radiation in the 1450Å - 1600Å band. The front surface of the instrument has vacuum integrity, thus permitting UV calibration when the instrument is mounted in the payload.

The calibration lamp optical system reflects the output flux onto the detector. The mirrors are optically-polished aluminum overcoated with magnesium fluoride optimized for maximum reflection in the 1400Å region.

The instrument electronic block diagram is shown in Figure 3.14. The output current is fed into a log amplifier capable of four (4) decades of data compression. The voltage output signal is then sent to the diode electronic chassis where it is scaled and formatted for transmission to onboard telemetry.

3.4 EXCEDE II Quick Look Data Evaluation

The UV-Visible Spectrometer system consists of two Ebert-Fastie scanning spectrometers and two wide band UV photodiodes. Instrument specifi-

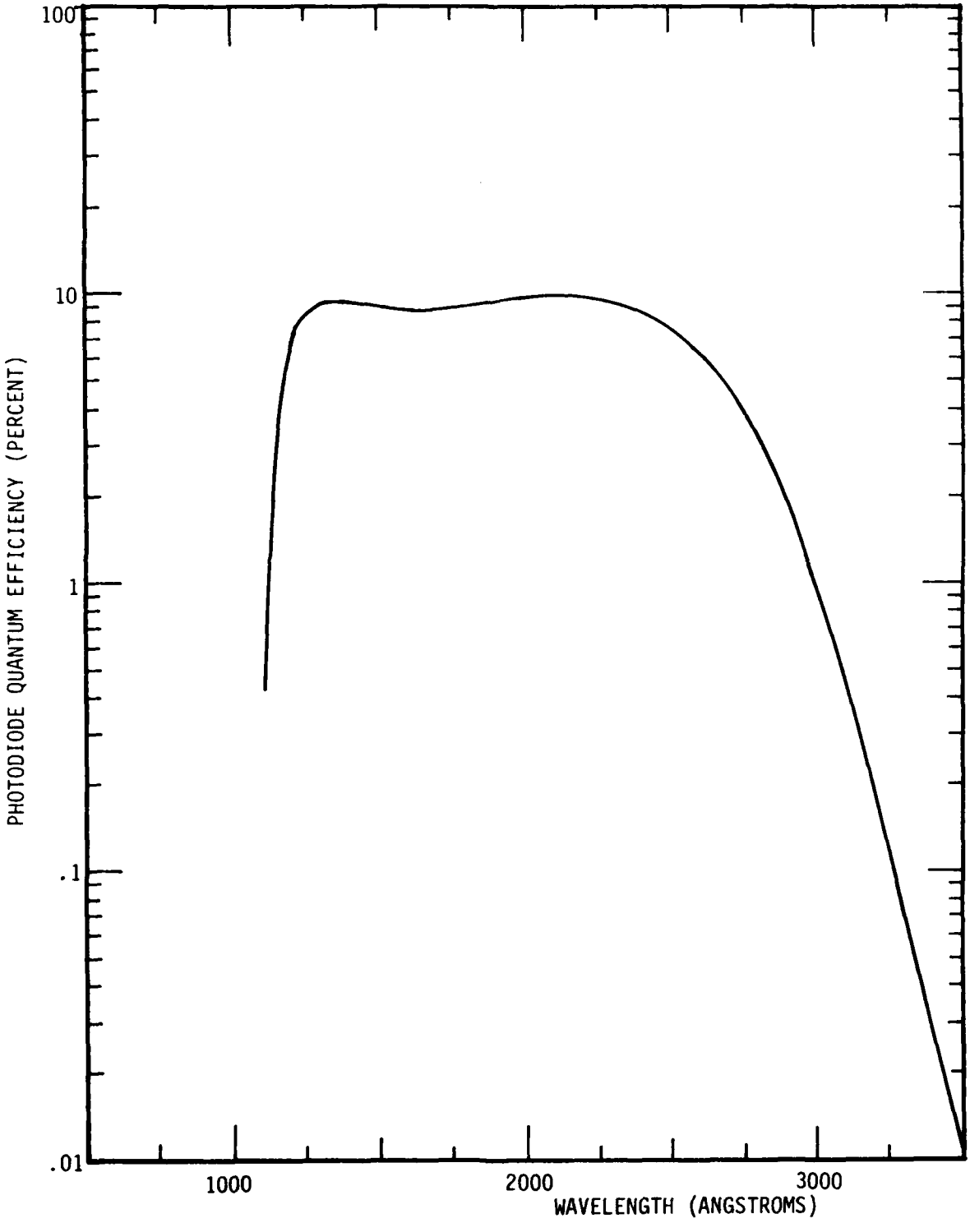

FIGURE 3.13 UV-1 DIODE SPECTRAL RESPONSE

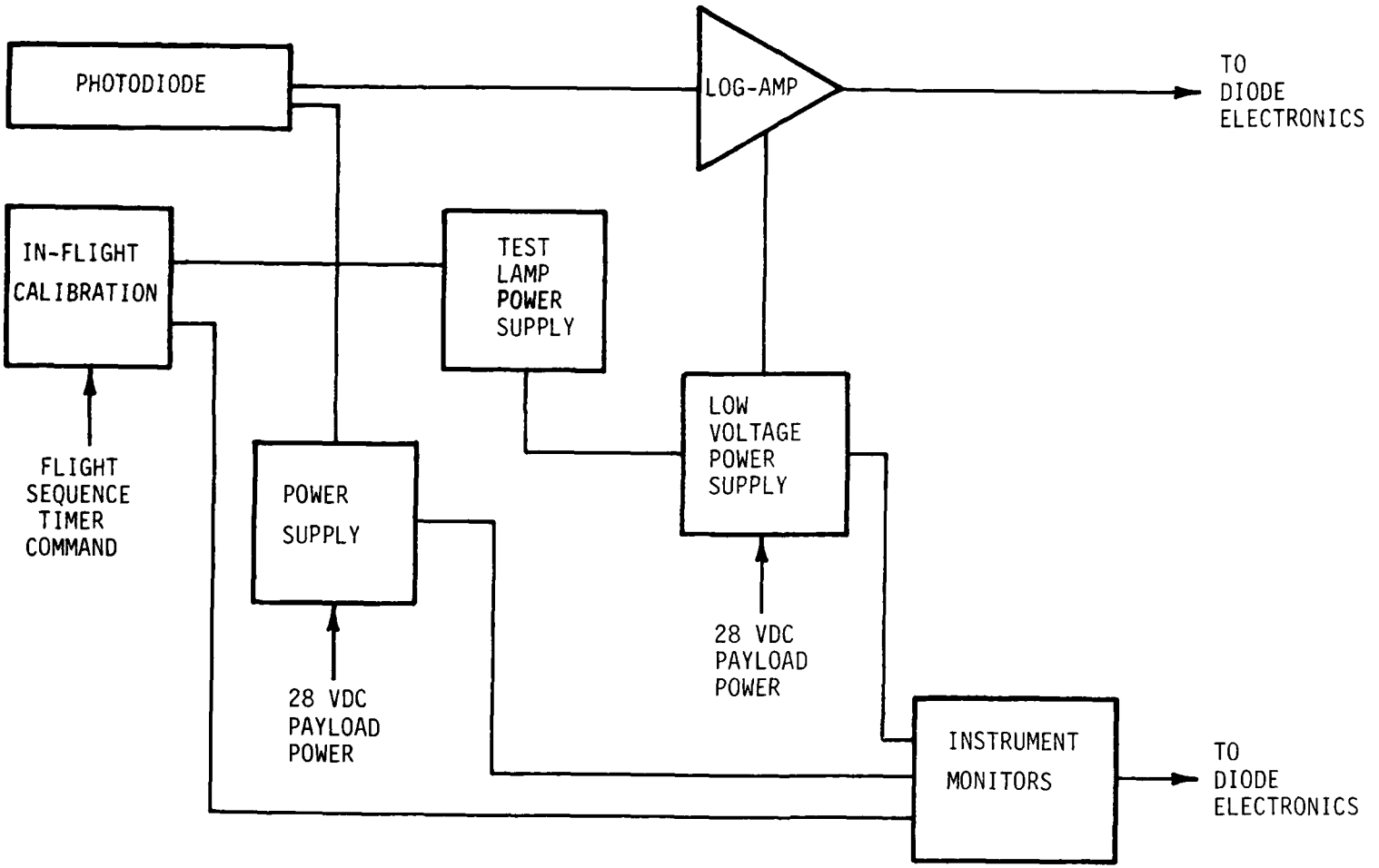

FIGURE 3.14 UV DIODE ELECTRONICS

cations are given in the previous sections. The system was aboard the EXCEDE II payload, EX851.44-1, which was launched from PFRR at 2002 on 28 October 1978.

Prelaunch and in-flight telemetry checkouts indicated that the spectrometer system was operational. No data were obtained because of a failure of the Space Data Corp. payload instrument door to eject.

During flight both the UV and Visible Spectrometer PCM data were monitored on an oscilloscope. During the flight no signals significantly greater than dark counts were observed. Data drop-outs, which have been attributed to telemetry, were observed through the flight. A complete reduction of the flight PCM data is planned.

The UV diodes, UV-1 and UV-2, also operated throughout the flight but no data were observed. The internal calibration was commanded by the payload timer at T-31 seconds but the calibration lamp power operated properly for only seconds. This problem would not have affected diode data acquisition.

For this summary, only the real-time strip chart data were used. In excess of thirty data drop-outs, ranging in duration from 100 msec to 6 seconds, were observed in the UV-1 and UV-2 diode data. These have been attributed to the telemetry system and are not tabulated.

It was requested that a glitch survey of the flight data be performed for diagnostic purposes. Table 3.12 gives the results of this survey.

TABLE 3.12
SURVEY OF UV DIODE FLIGHT DATA

T+31 seconds	Diode Calibration 1 Starts
T+38.8 seconds	Diode Calibration Power Supply Malfunction
T+55.2 seconds	Diode Calibration 1 End -
T+61.0 seconds	Diode Calibration 2 Start -
T+64.9 seconds	Diode Calibration 2 End
T+74.0 seconds	Transient of Approximately 20 msec duration observed on UV-1 and UV-2 Data
T+78.4 seconds	Large transient (28 volts) with a very slow decay observed on UV-1. A smaller (~1 volt) transient is on the UV-2 data
T+88 seconds	UV-1 data has returned to pre-transient zero levels
T+259 seconds	Diode Calibration 3 Starts
T+264 seconds	Diode Calibration 3 Ends
T+273 seconds	20 msec transient on UV-1 Data
T+378 seconds	End of Data (LOS).

4.0 AURORAL ELECTRON MEASUREMENTS - ROCKET IC819.08-1

4.1 Introduction

Previous nighttime measurements have indicated that bright auroral arcs are produced by localized enhancements in electron energy and flux deposited in the upper atmosphere and that this localized enhancement is inbedded in an extended weaker deposition which fills much of the auroral zone. The primary instrument for electron flux measurements during the ICECAP Program was a Visidyne electron electrostatic analyzer (ESA). Measurements with this instrument on Rocket 18.219-1 showed the energy of the peak electron flux was in excess of 30 Kev, the instrument cutoff. In order to extend the measurements to higher energies it was decided to fly two instruments with overlapping energy ranges from 2 Kev to 30 Kev (ESA 202B) and 5 Kev to 42 Kev (ESA 211). In future flights the high energy analyzer range will be extended to 50 Kev.

4.2 Electrostatic Analyzer Design

The electrostatic analyzer consists of a pair of spherical octants. An exponentially decreasing positive voltage is applied to the inner plate. The outer plate is at ground potential. Electrons entering between the plates with the proper angle and energy will pass through the plates without striking either plate surface. Electrons passing through the analyzer plates strike an aluminum-covered scintillator coupled to a photomultiplier. For the low energy instrument, an accelerating voltage is applied to the aluminum deposition to increase the signal produced by low energy electrons. In the high energy instrument, no voltage is applied to the aluminum deposition. The output signal of the photomultiplier is then a measure of the electron flux at energy E, where E is the energy at the center of the energy band for the applied voltage, V. For this instrument, the geometrical parameters are such that $E = 10\ V$. The angular field of view of the instrument is 6.4 degrees by 16 degrees and the geometric factor is 4.6×10^{-2} cm^2-sr. The applied plate signal is an exponentially decreasing voltage. The energy response of the instrument is verified by vacuum testing with a variable electron beam (1 - 6 Kev).

In order to improve the instrument signal to noise, the exponential sweep applied to the analyzer plate is modulated with a 1 kilohertz square wave. The output of the photomultiplier is detected by a narrow band amplifier tuned to the frequency used to modulate the analyzer plate voltage. At plate voltages below 400 volts, there is some distortion of the modulating square wave on the analyzer plate.

The scintillator used in this instrument is calcium fluoride (europium activated). Two thin layers of aluminum are vacuum deposited on the scintillator to reduce light sensitivity and to provide a conducting surface on which to apply an accelerating voltage. The thickness is measured by the interferometric step wedge technique. To prevent the analyzer plate voltage from effecting vehicle potential, a grounded double grid is located in front of the analyzer entrance aperture.

In reducing the low energy electron data, it is necessary to take into account the energy loss in the aluminum.

The incident electron flux is calculated from the following formula:

$$N_{(E)} = \frac{I - I_n}{S\varepsilon e(A\Omega)\ \Delta E\beta(E + eV_{PA} - 1.3\ E_c)}$$

where:

$N_{(E)}$ $\{cm^2 sec\ sr\ ev\}^{-1}$	Incident electron flux at energy E.
I {amp}	Photomultiplier current measured at plate voltage V corresponding to electron energy bandpass centered at E.
S {amp watts^{-1}}	Scintillator and photomultiplier response (α-ray source).
ε	Energy dependent correction of scintillator response for electron deposition (Fig. 4.1).
e {coulombs}	Electron charge 1.6×10^{-19} coulombs.

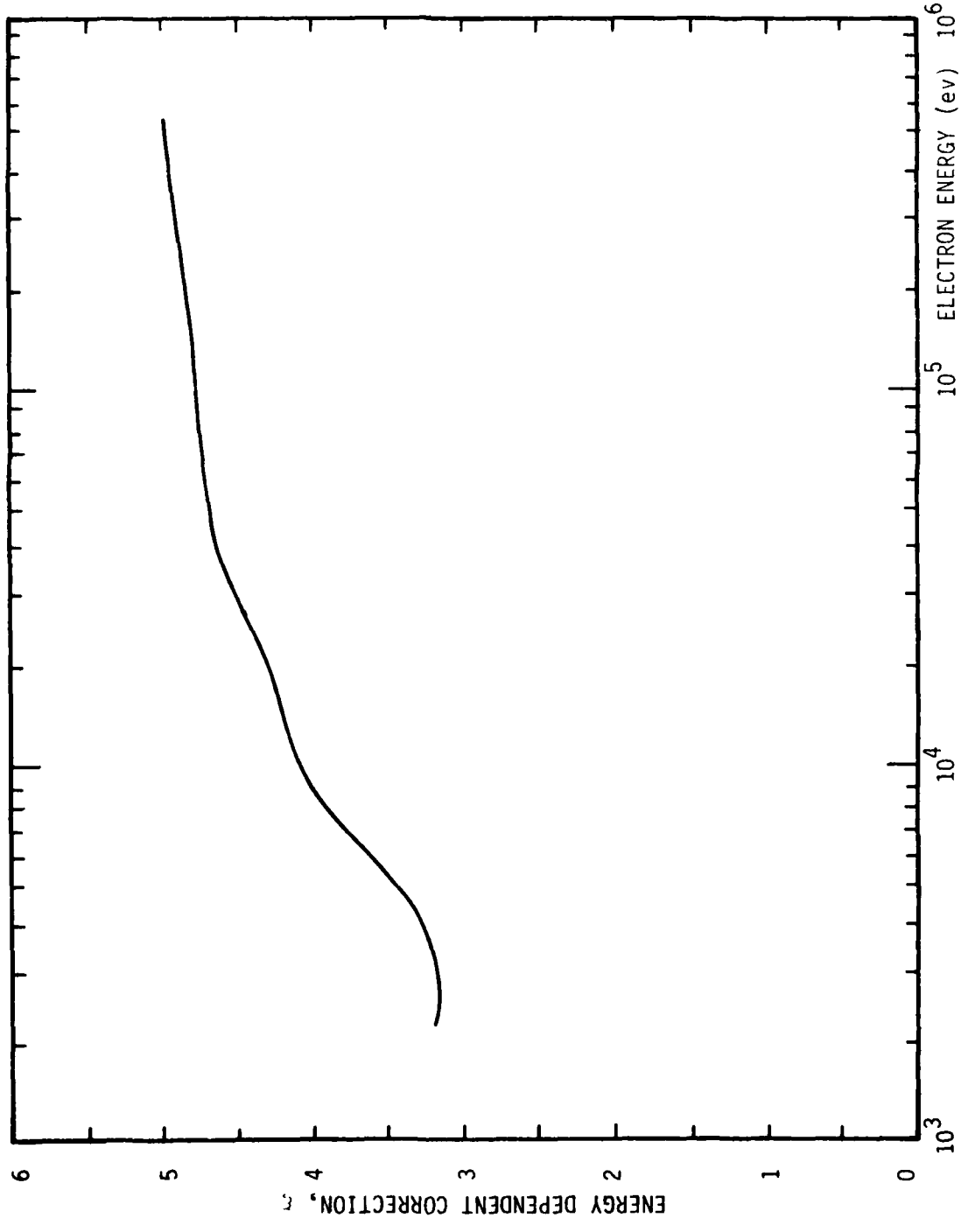

FIGURE 4.1 ENERGY DEPENDENT CORRECTION OF SCINTILLATOR RESPONSE VS. ELECTRON ENERGY

$A\Omega$ {$cm^2 sr$}	Instrument geometric factor multiplied by grid transmission.
ΔE {electron volts}	Electron energy bandpass, FWHM.
E	Electron energy at center of bandpass.
β	Correction for loss by backscattering from the scintillator[5].
V_{PA}	Post Accelerator Voltage.
I_n	Analyzer noise current.
E_c {electron volts}	Critical energy - the energy of an electron with practical range equal to thickness of aluminum deposition (Fig. 4.2[6]).

The geometric factor and energy bandpass have been experimentally measured in the laboratory. The scintillator and photomultiplier sensitivity, S, is determined by measuring the combined response of the scintillator and photomultiplier to a known source of radiation. In this case, an americium 241 source (5.5×10^6 ev alpha particles) is placed in contact with the calcium fluoride (europium activated) scintillator and the photomultiplier output current is measured at the normal photomultiplier operating voltage. The measured response for alpha particles is multiplied by ε (Figure 4.1) to correct for the higher scintillator response to electron deposition [7]. In calculating the energy dependence of ε, we have taken into account the average loss in the aluminum foil.

4.3 Calibration Data

4.3.1 ESA 202B

The characteristics of this instrument are summarized as follows:

Electron Energy - 2 keV to 30 keV

Energy Resolution - 12% FWHM

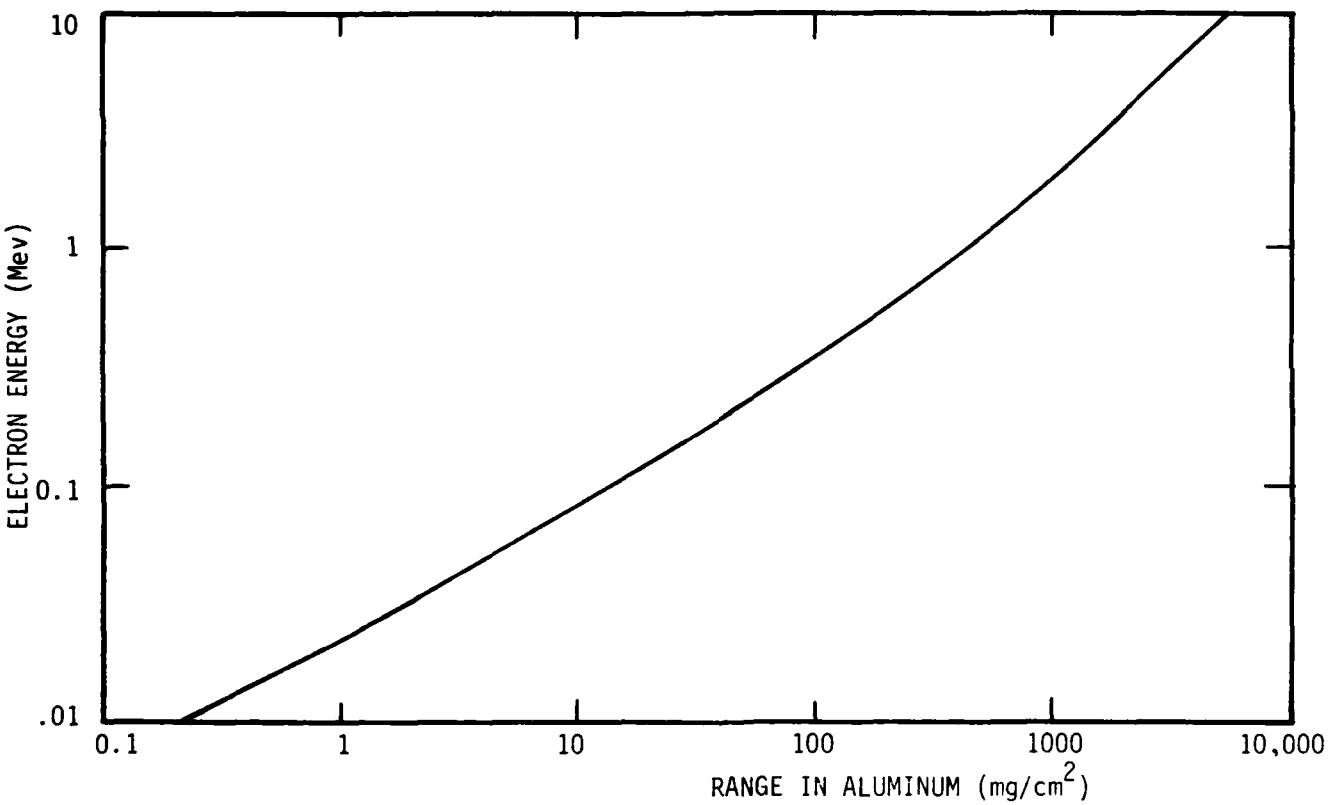

FIGURE 4.2 ELECTRON ENERGY VS. RANGE IN ALUMINUM

Angular Field of View - $6.4^{o} \times 16^{o}$

Geometric Factor ($A\Omega$) - $9.3 \times 10^{-2} cm^{2}$-sr

Look Angle - 45^{o} elevation from rocket axis, 0^{o} azimuth

S (Scintillator and PMT Response)- 48.2 amp-watt^{-1} (measured with .68 μcurie Am 241 source)

Instrument Light Sensitivity - 2.8×10^{-10} amp - (ft -candle)$^{-1}$

Aluminum Coating Thickness - 1140 ± 50Å

Sweep Period - 540 milliseconds

Sweep Time Constant - 94 milliseconds

Calibration data curves for this instrument are given in Figures 4.3 to 4.10. The sweep voltage monitor output signal is approximately 1 volt per 1 kv on the analyzer plate. Figure 4.7 gives the plate monitor output voltage as a function of plate voltage. The monitor voltage rise time is slower than the sweep voltage rise time. For this reason, the monitor voltage should not be used for calibration for times less than 50 milliseconds after the start of the sweep. The calibration data for times less than 50 milliseconds after the start of the analyzer voltage sweep are given in Figure 4.6. Electron energy versus sweep time for times greater than 50 milliseconds is given in Figure 4.5.

The instrument was flown with the post accelerator operated at a voltage of 2.71 kv. The post accelerator monitor voltage as a function of post accelerator voltage is given in Figure 4.8.

The sweep calibration is given in Table 4.1 and the data points monitored to verify proper instrument performance are listed in Table 4.2.

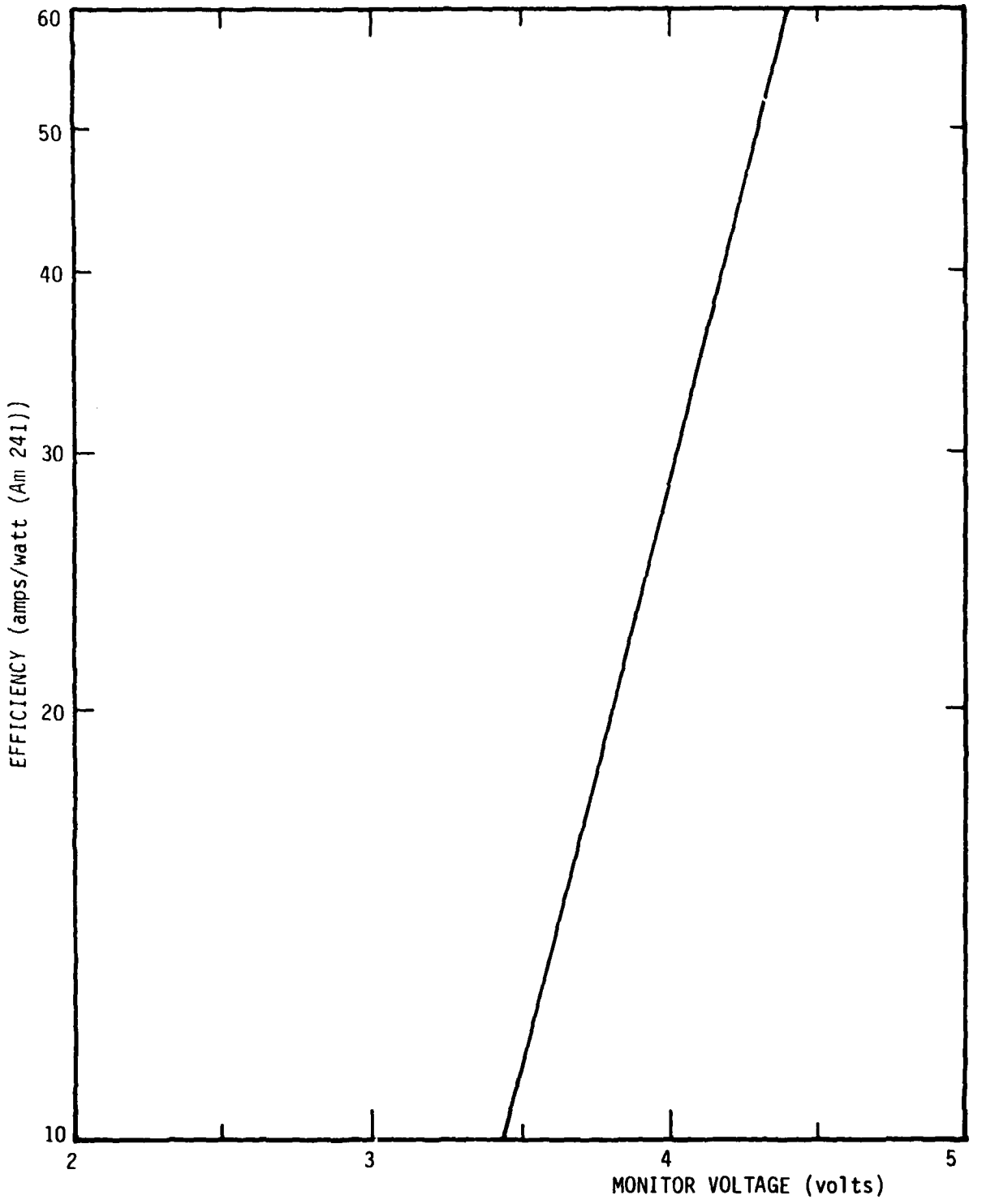

FIGURE 4.3 ESA 202B, PMT SCINTILLATOR EFFICIENCY VS.
PMT HIGH VOLTAGE MONITOR VOLTAGE

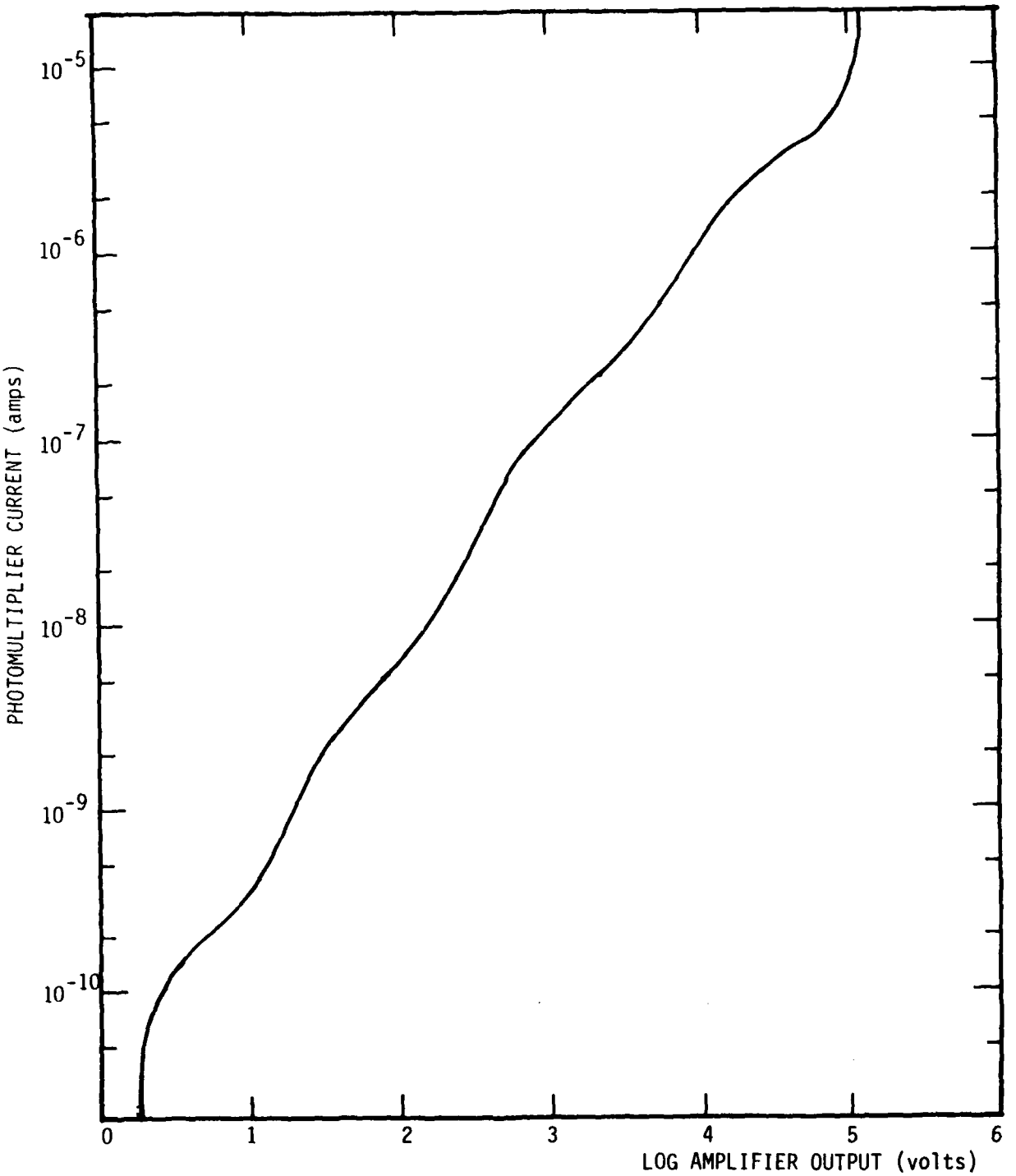

FIGURE 4.4 ESA 202B, LOG AMPLIFIER CURRENT-VOLTAGE CALIBRATION

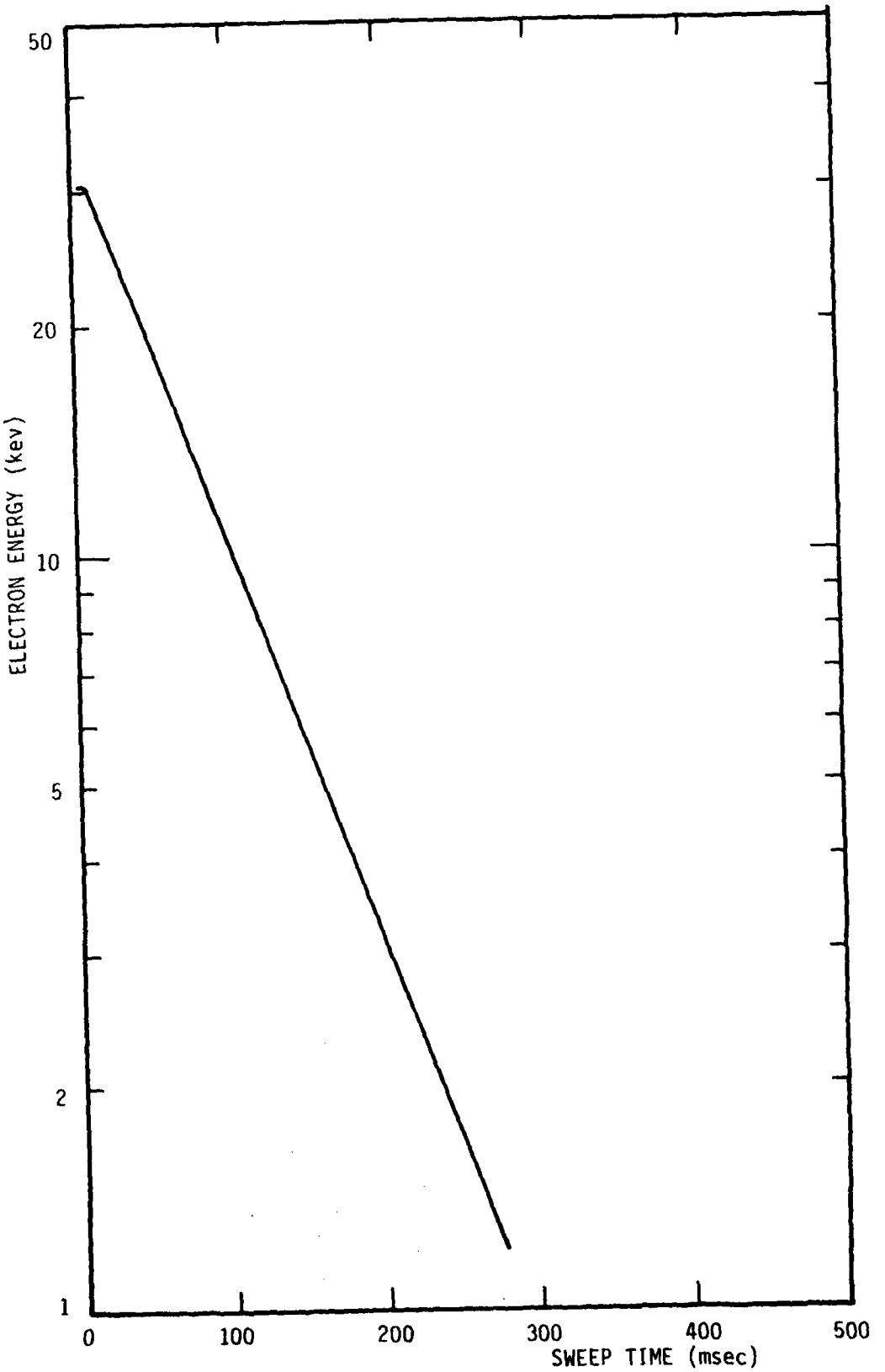

FIGURE 4.5 ESA 202B, ELECTRON ENERGY VS. SWEEP TIME

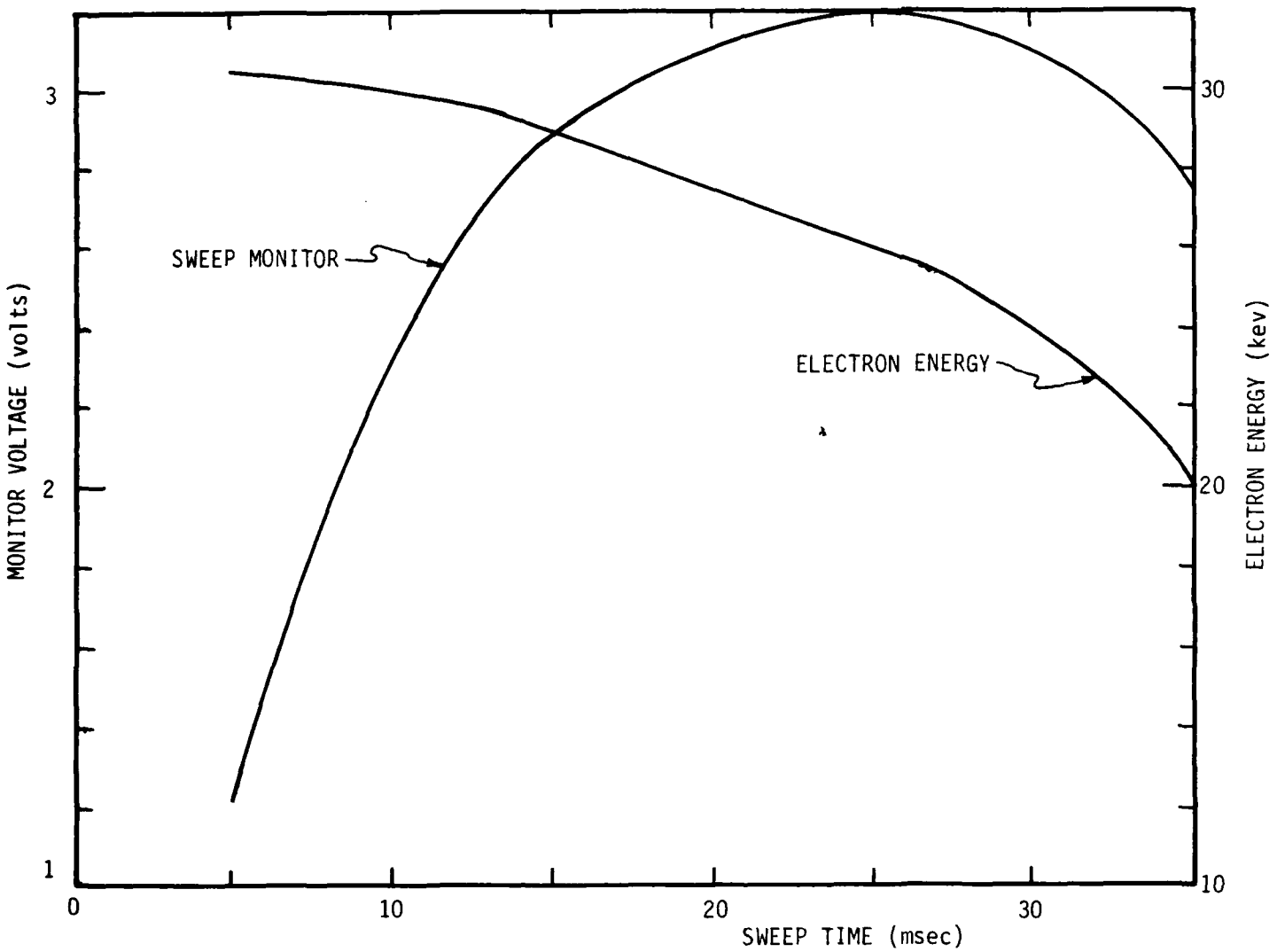

FIGURE 4.6 ESA 202B, SWEEP CALIBRATION, T < 35 msec

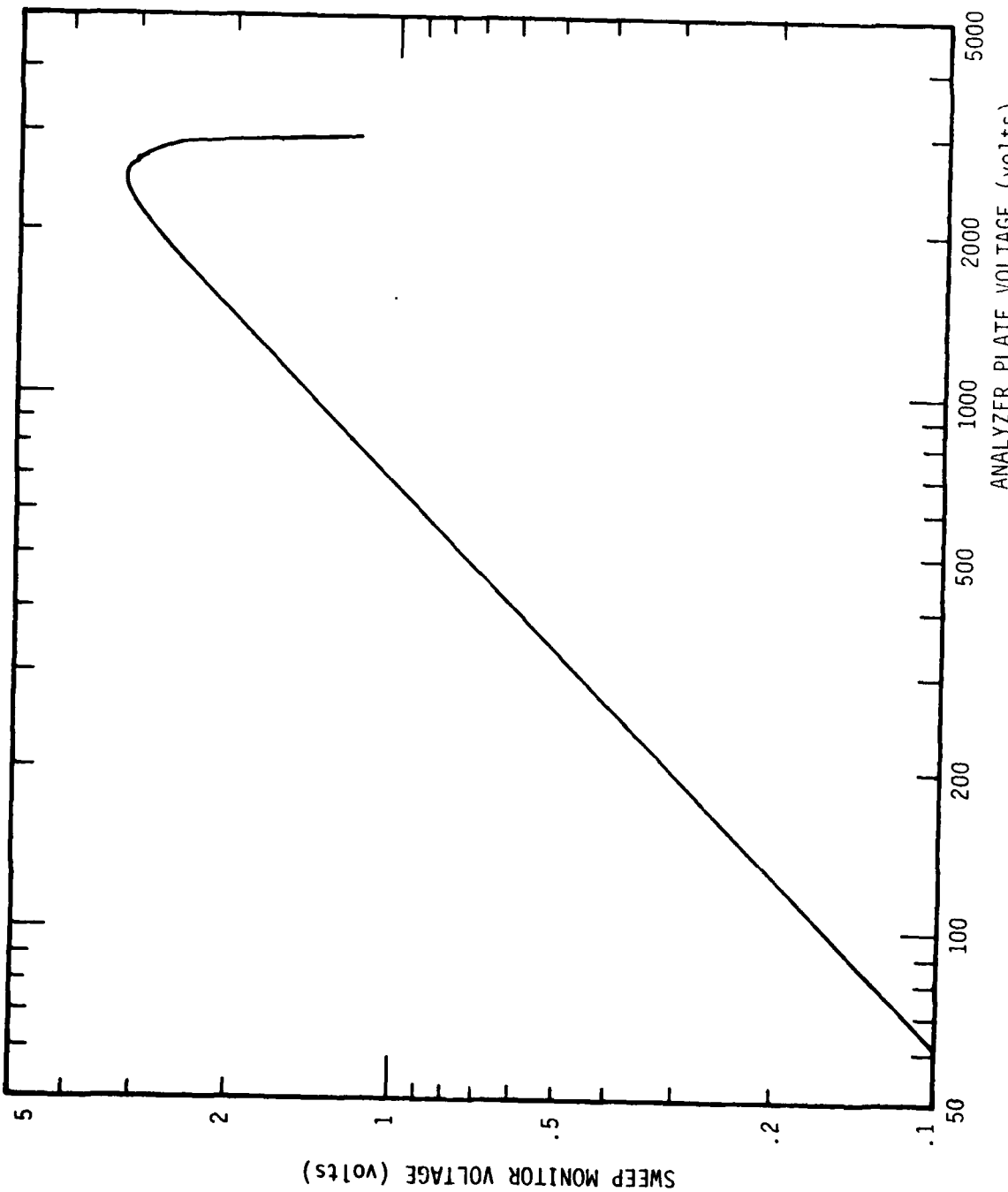

FIGURE 4.7 ESA 202B, ANALYZER SWEEP VOLTAGE VS. SWEEP MONITOR VOLTAGE

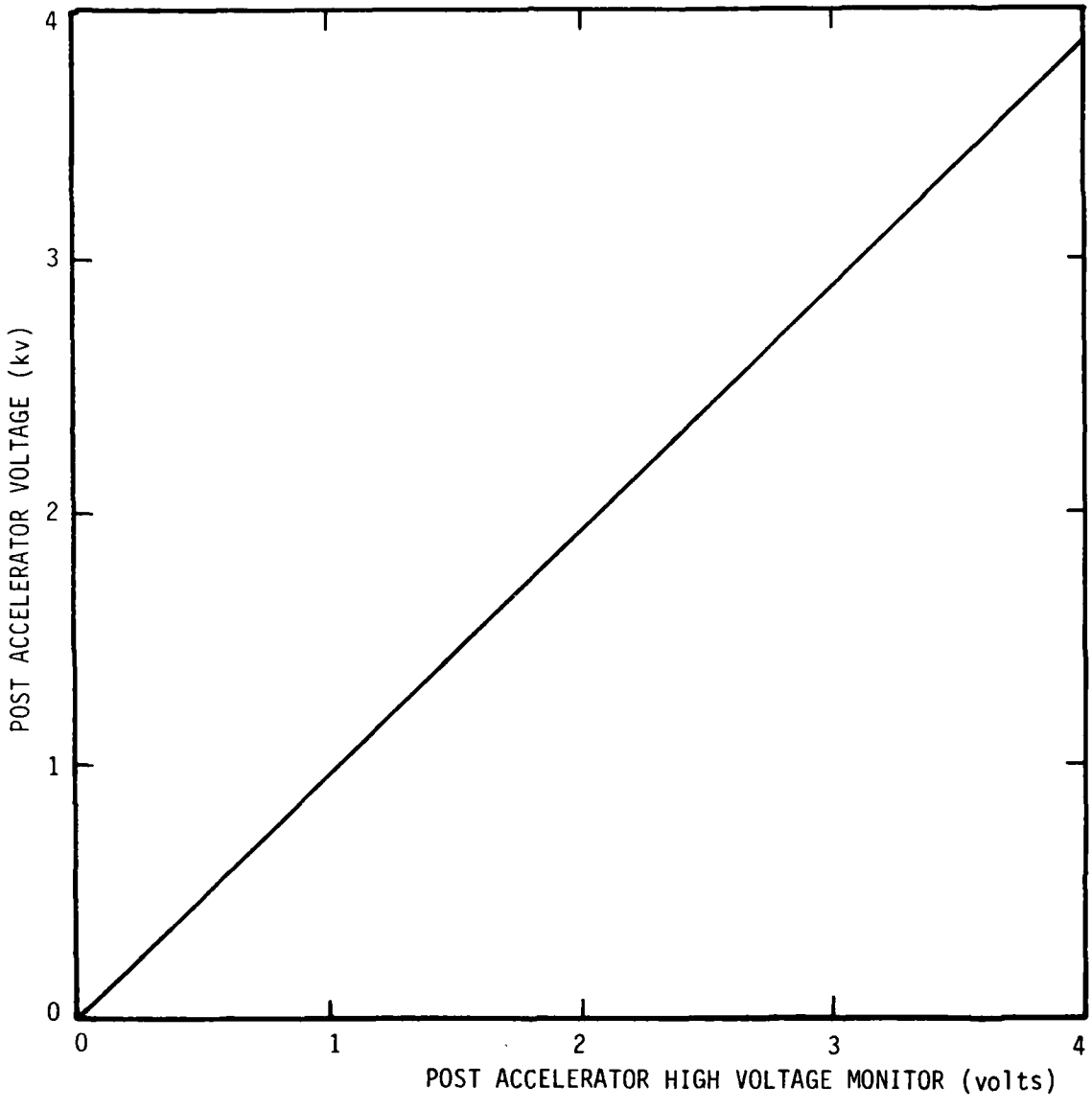

FIGURE 4.8 ESA 202B, POST ACCELERATOR HIGH VOLTAGE VS. MONITOR VOLTAGE

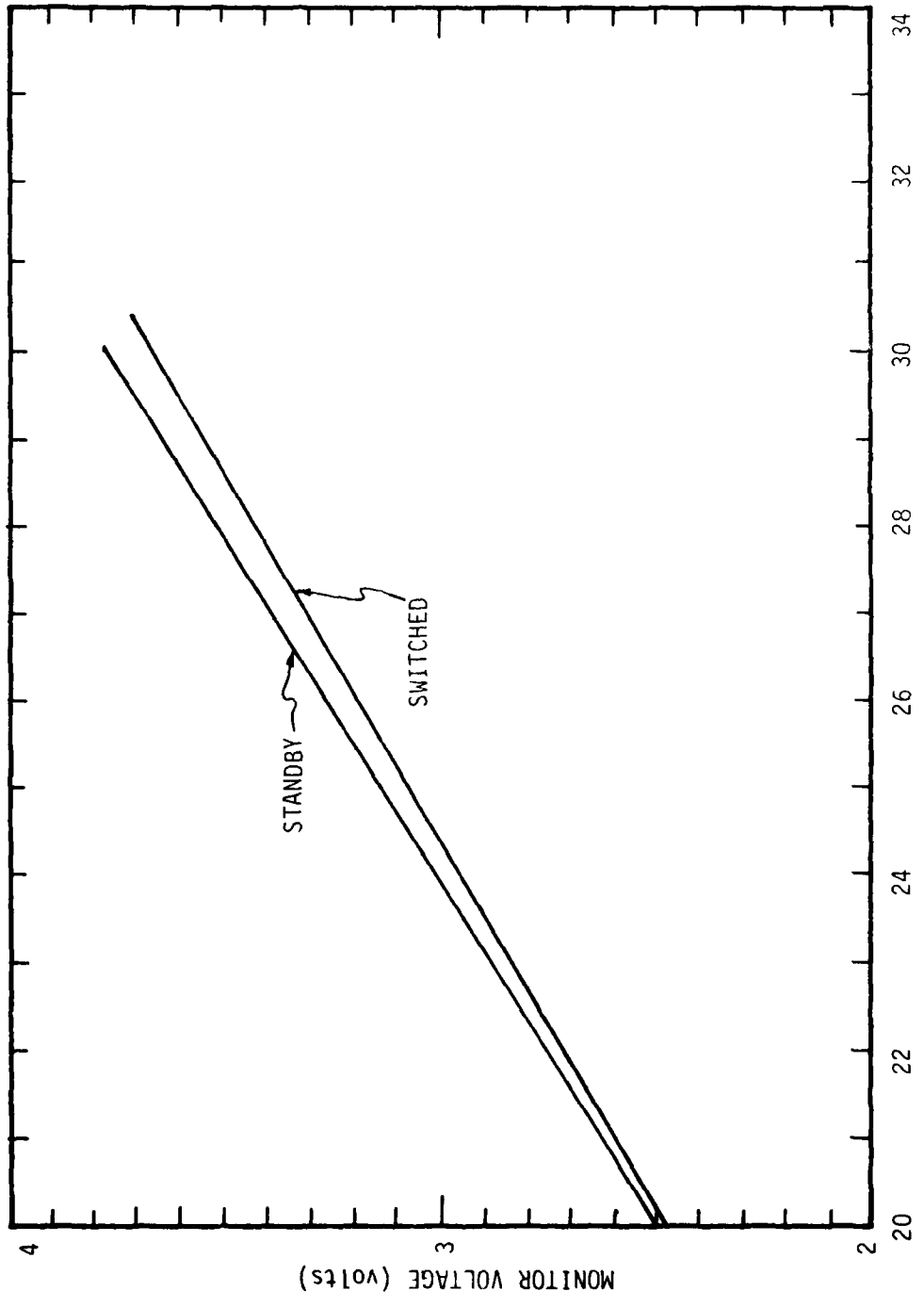

FIGURE 4.9 ESA 202B, +28 VDC MONITORS

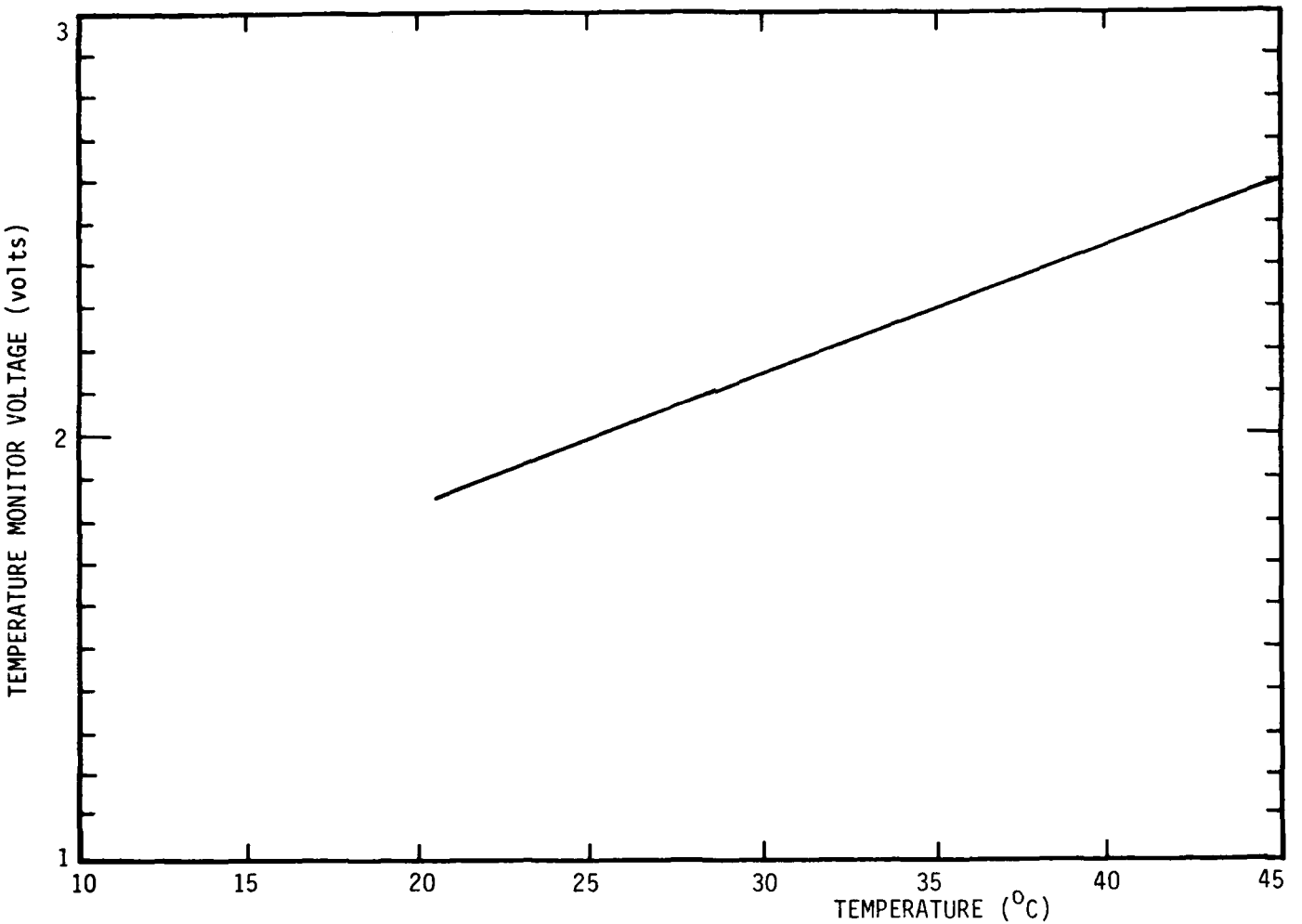

FIGURE 4.10 ESA 202B, TEMPERATURE MONITOR

TABLE 4.1

ESA 202 B SWEEP CALIBRATION

Time (msec)	Sweep Mon. (volts)	H/V (kv)	Electron Energy (kev)
0	0	0	0
5	1.20	3.05	30.5
10	2.30	3.00	30.0
15	2.90	2.90	29.0
20	3.10	2.75	27.5
25	3.20	2.60	26.0
35	3.10	2.40	24.0
50	2.75	2.00	20.0
75	2.00	1.40	14.0
100	1.50	1.02	10.2
125	1.1	0.78	7.8
150	0.82	0.56	5.6
175	0.62	0.43	4.3
200	0.47	0.33	3.3
225	0.35	0.23	2.3
250	0.26	0.17	1.7
275	0.18	0.12	1.2
300	0.11	0.06	0.6

TABLE 4.2

ESA 202 B COMMUTATOR DATA

Commutator Point	Function	Function Value	Monitor Voltage (volts)
31	Zero Voltage	0.0 vdc	0.0
32	28 vdc Switched	28 vdc	3.42
33	28 vdc Standby	28 vdc	3.52
34	+15 vdc	+14.8 vdc	3.48
35	-15 vdc	-14.8 vdc	2.38
36	PMT HV	2.75 kv	4.28
37	PA HV	2.71 kv	2.64
38	Cover Position	Cover On	0.61
		Cover Off	3.83
39	Temperature	22^{o} C	1.95
40	Zero Voltage	0.0 v	0.0

4.3.2 ESA 211

The characteristics of this instrument are summarized as follows:

Electron Energy - 5 kev to 42 kev
Energy Resolution - 11% FWHM
Angular Field of View - $6.4^{o} \times 16^{o}$
Geometric Factor ($A\Omega$) - $4.6 \times 10^{-2} cm^{2}$-sr
(corrected for grid transmission)
Look Angle - 45^{o} elevation from rocket axis,
180^{o} azimuth
S (Scintillator and PMT Response) - 23.6 amp-watt^{-1}
Instrument Light Sensitivity - 5.9×10^{-12} amp -
(ft.-candle)$^{-1}$
Aluminum Coating Thickness - 1100 ± 50Å
Sweep Period - 530 milliseconds
Sweep Time Constant - 90 milliseconds

Calibration data curves for this instrument are given in Figures 4.11 to 4.16. Electron energy versus sweep time for times greater than 25 milliseconds is given in Figure 4.13.

The instrument was flown with the post accelerator operated at a voltage of 20 volts. Figure 4.15 shows the post accelerator monitor voltage as a function of post accelerator voltage.

The sweep calibration is given in Table 4.3 and the data points monitored to verify proper instrument performance are listed in Table 4.4.

4.4 Rocket IC819.08-1 Data and Engineering Evaluation

Rocket IC819.08-1, a multi-instrument payload on a Sergeant-Hydac rocket, was launched at 8:10:50 UT on 28 February 1978 from the Poker Flat Research Range. Included in the instrumentation were two electrostatic analyzers (ESA) designed and fabricated by Visidyne, Inc. These instruments are described in detail in the preceding sections. One

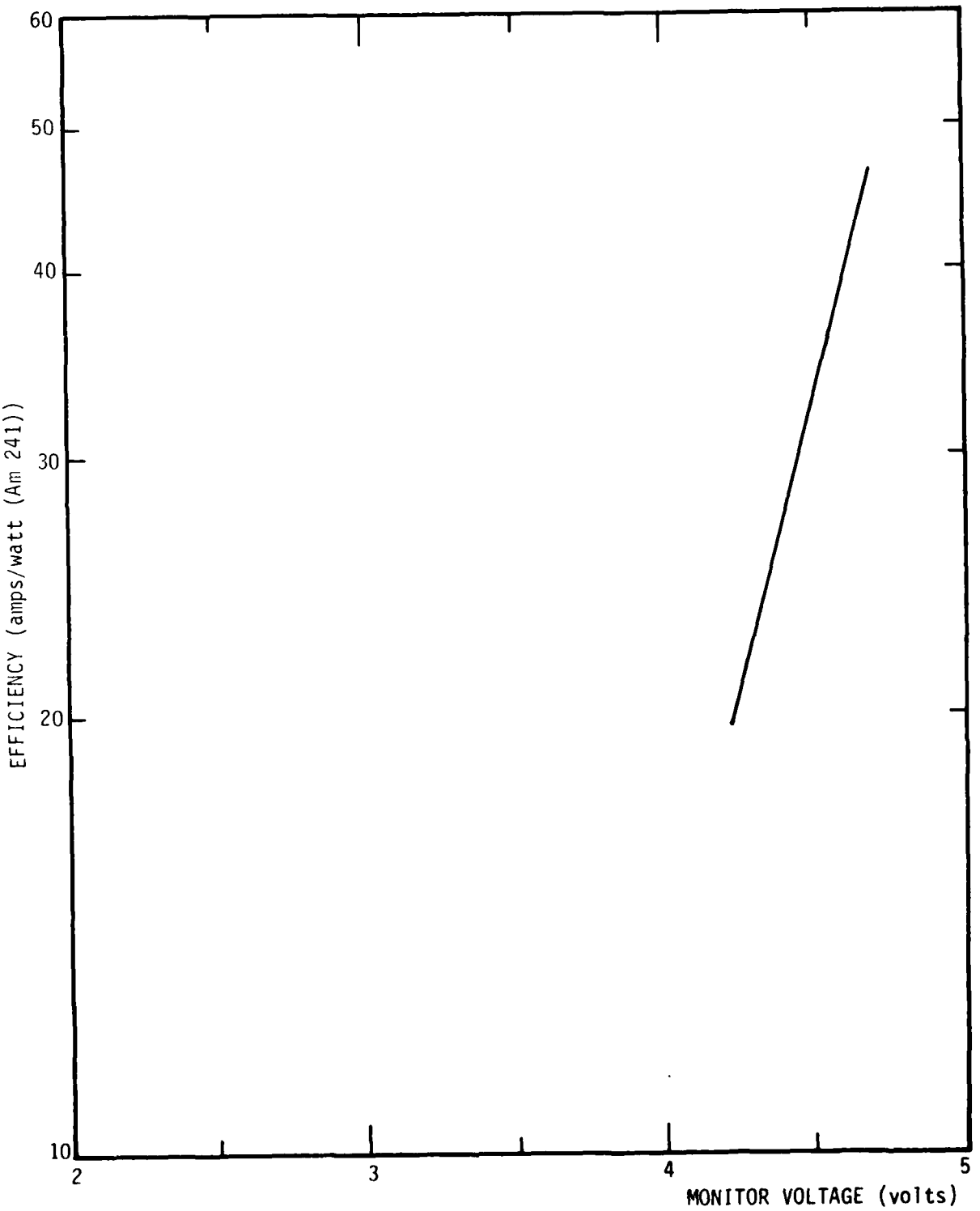

FIGURE 4.11 ESA 211, PMT SCINTILLATOR EFFICIENCY VS. PMT HIGH VOLTAGE MONITOR VOLTAGE

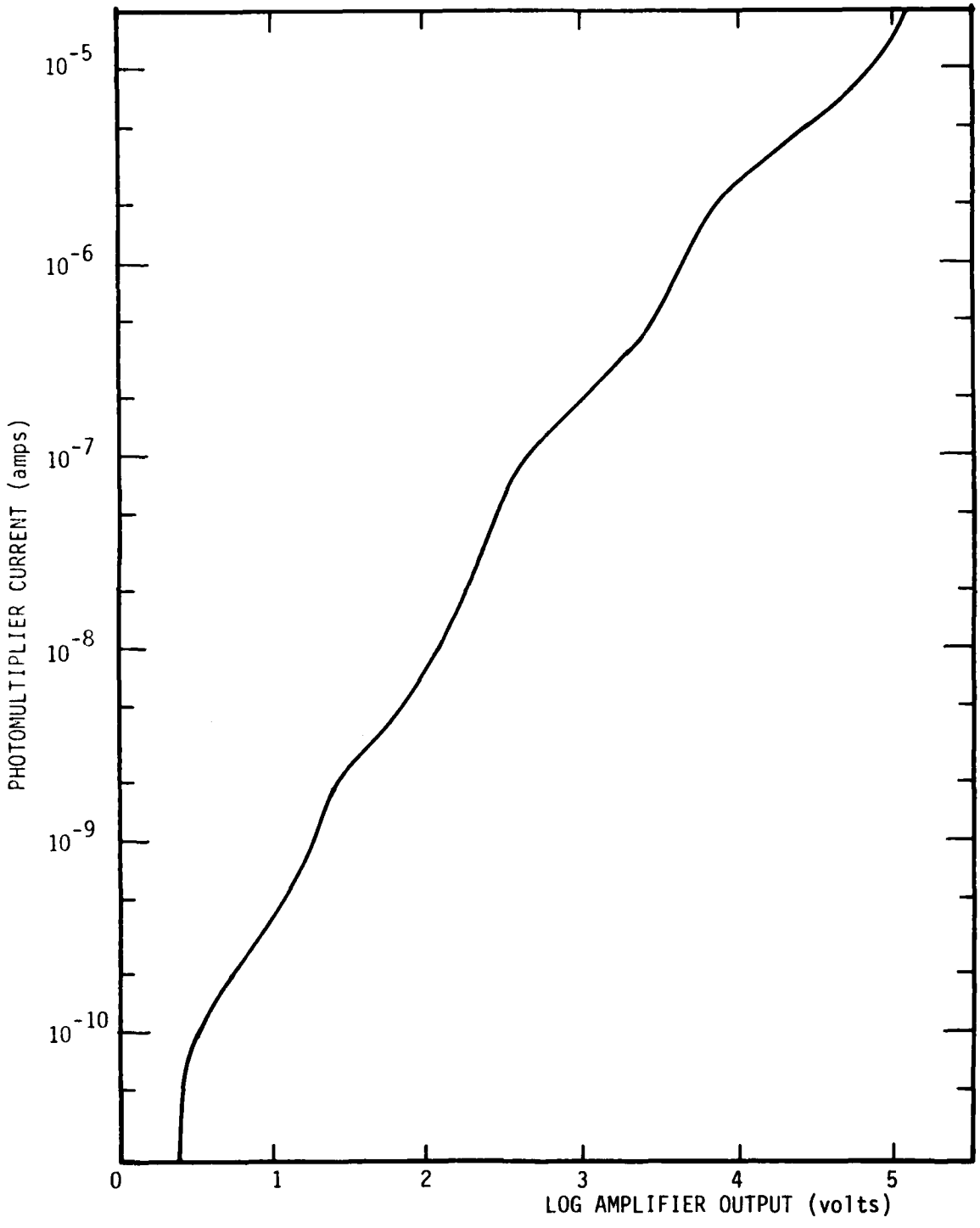

FIGURE 4.12 ESA 211, LOG AMPLIFIER CURRENT-VOLTAGE CALIBRATION

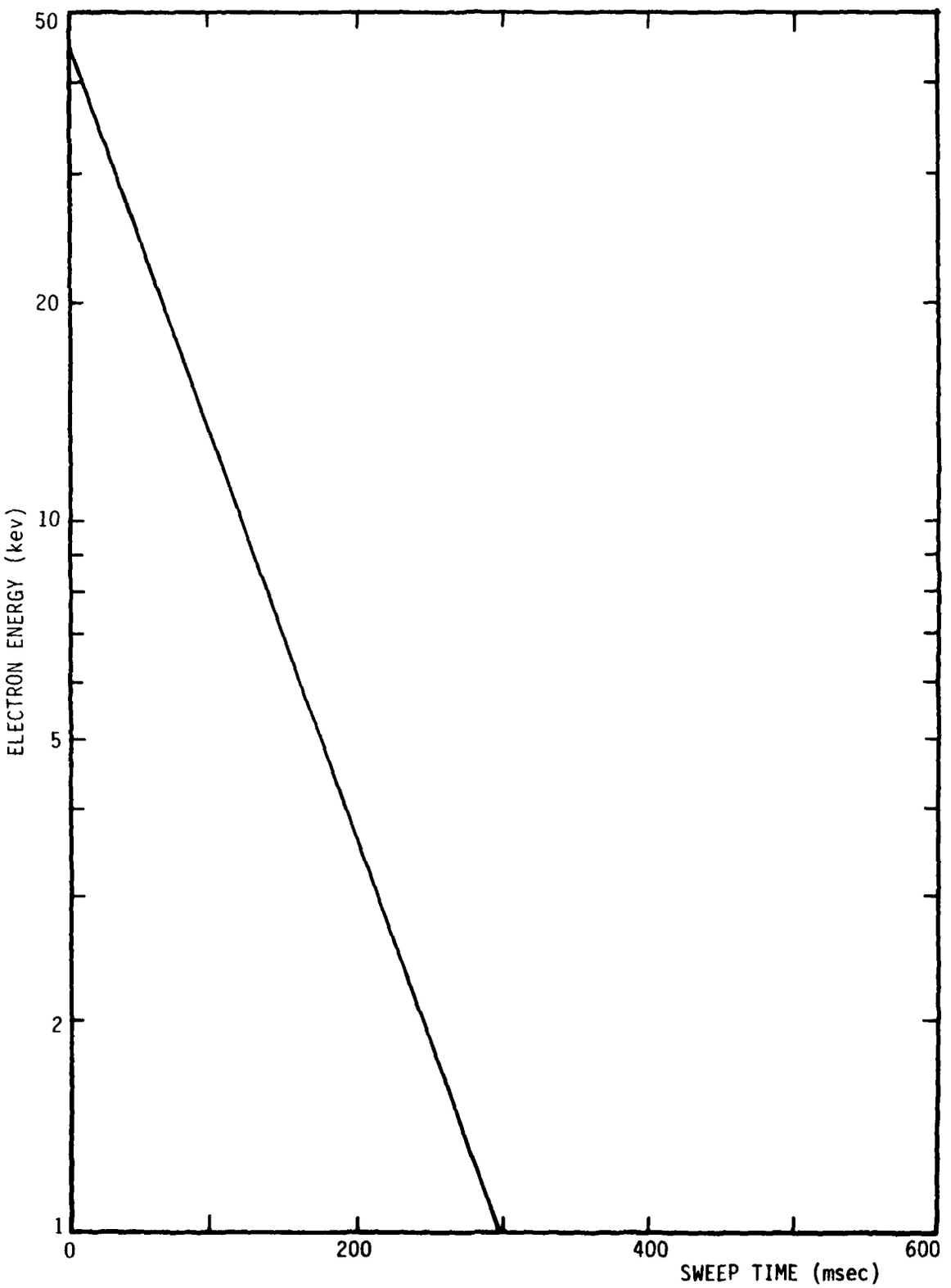

FIGURE 4.13 ESA 211, ELECTRON ENERGY VS. SWEEP TIME

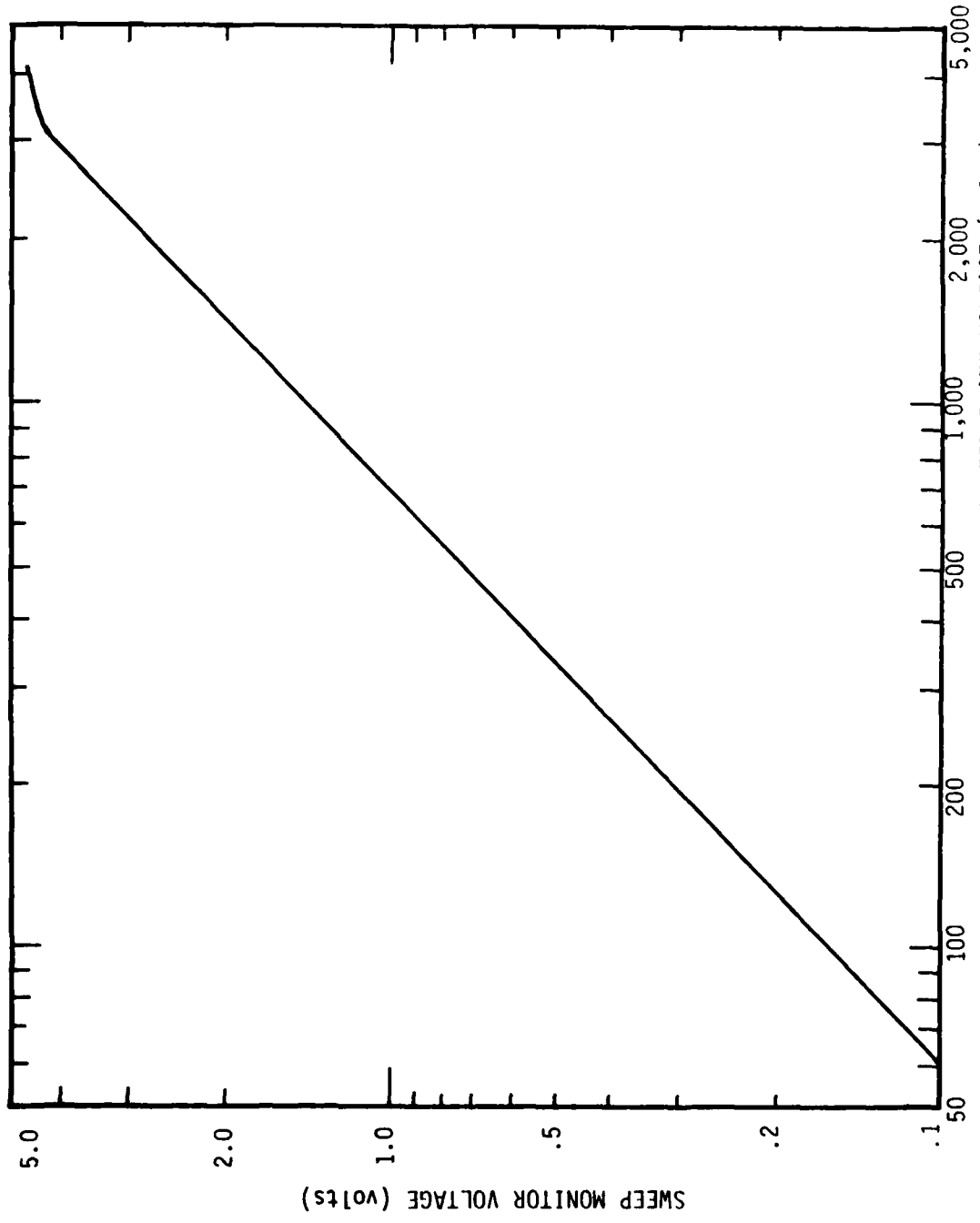

FIGURE 4.14 ESA 211, ANALYZER SWEEP VOLTAGE VS. SWEEP MONITOR VOLTAGE

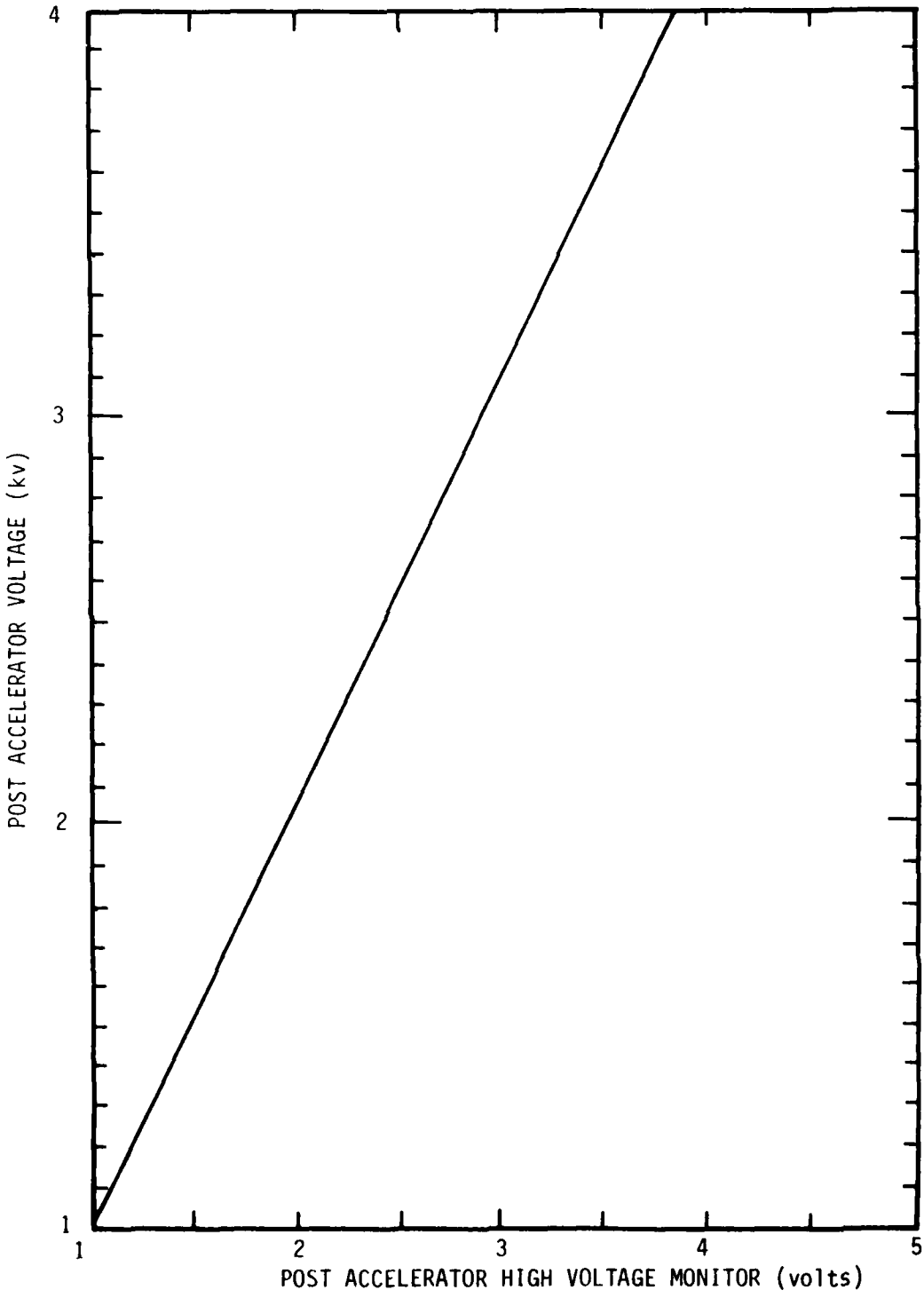

FIGURE 4.15 ESA 211, POST ACCELERATOR HIGH VOLTAGE VS. MONITOR VOLTAGE

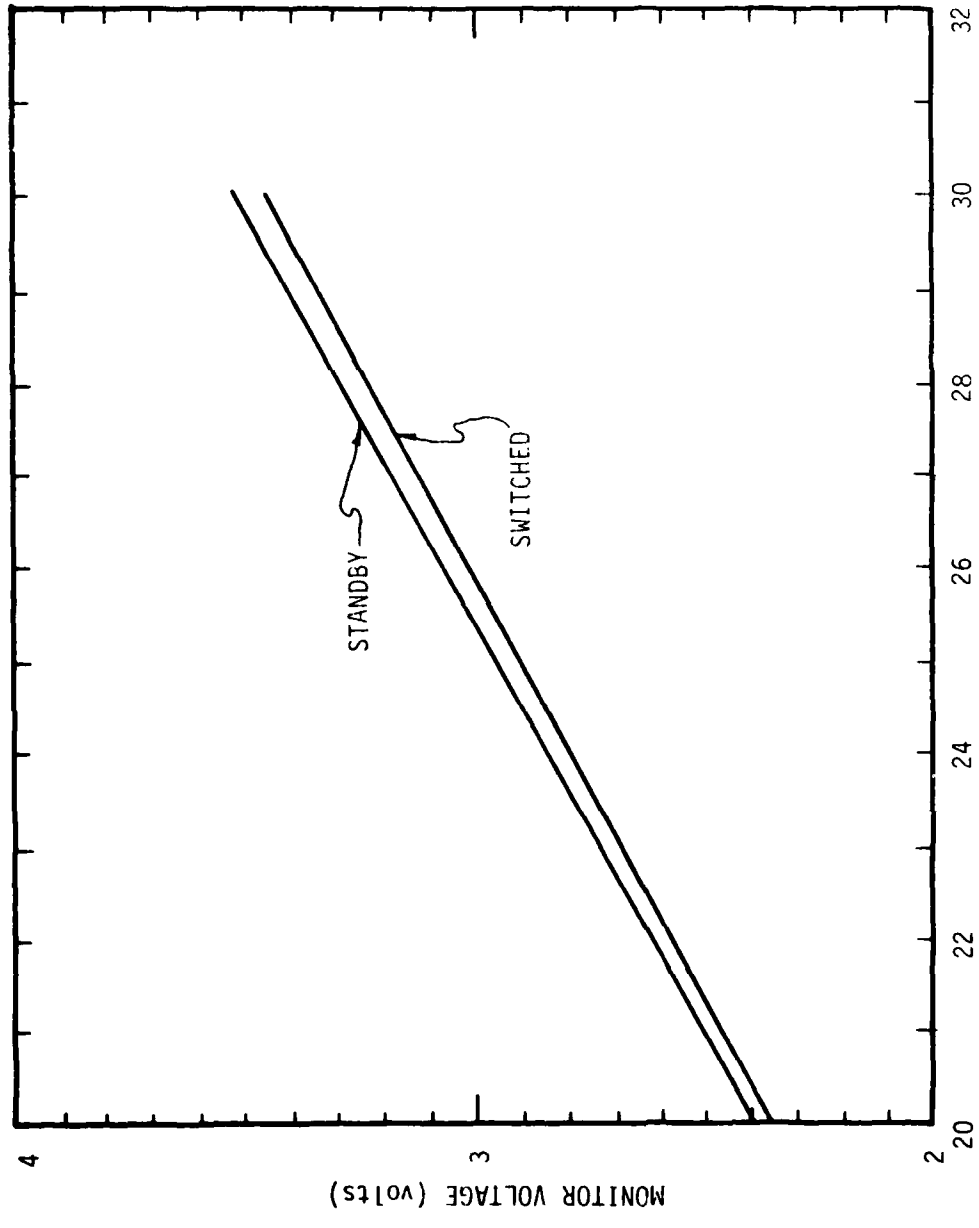

FIGURE 4.16 ESA 211, +28 VDC MONITORS

TABLE 4.3

ESA 211 SWEEP CALIBRATION

t msec	HV Mon Volts	H/V kv	E kev
7.5	4.7	4.2	42
32.5	4.35	3.2	32
50	3.30	2.40	24
75	2.60	1.85	18.5
100	1.85	1.35	13.5
125	1.35	0.96	9.6
150	1.00	0.68	6.8
175	0.68	0.48	4.8
200	0.47	0.34	3.4
225	0.32	0.26	2.6
250	0.23	0.16	1.6
275	0.15	0.10	1.0
300	0.10	0.06	0.06

instrument was essentially the same as that flown on previous rocket flights. The other instrument was a modified version to provide higher energy measurements up to 40 kev. Previously, the peak detectable energy was 30 kev.

On an earlier rocket flight (18.219-1), a payload had overflown an intense, rapidly moving auroral arc with a brightness of more than 125 KR at 5577Å. The data from the ESA in this payload were saturated at this point and it also appeared that the electron energy at peak intensity was greater than 30 kev.

Rocket IC819.08-1 overflew an even more intense auroral arc than did Rocket 18.219-1, as can be seen in Figure 4.17. The peak 5577Å brightness as measured by the ground based, meridan scanning photometers was greater than 200 KR. Preliminary data from the ESA at this point do not show any evidence of saturation. Examples of raw data taken during the rocket flight are shown in Figure 4.18. When this data is reduced, it will provide unique information about the electron energy spectra associated with intense auroral arcs.

TABLE 4.4
ESA 211 COMMUTATOR DATA

Function	Function Value	Monitor Voltage
Zero Voltage		
+28 DC Switched	28.0	3.24
+28 DC Standby	28.0	3.31
+15 VDC	+15	3.40
-15 VDC	-15	2.32
PM H/V	23.6 amps/watt (Am. 241)	4.37
PA H/V	0	0.03
Cover Position	Cover ON Cover OFF	0.61 4.23
Temperature	22.5^{o} C	1.98
Zero Voltage		

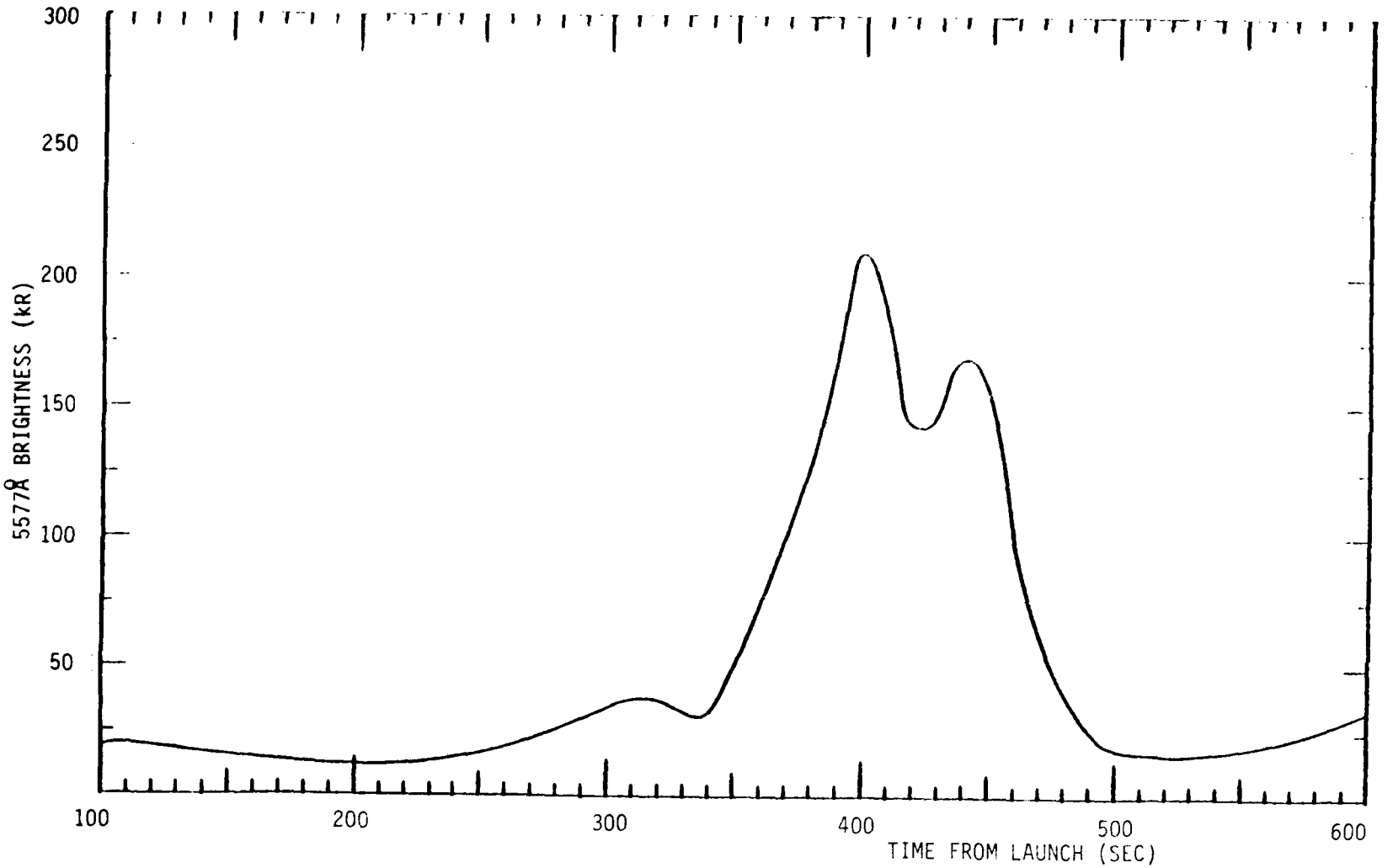

FIGURE 4.17 ROCKET IC 819.08-1 AURORAL BRIGHTNESS DOWN THE MAGNETIC FIELD LINE INTERCEPTED BY THE ROCKET PAYLOAD

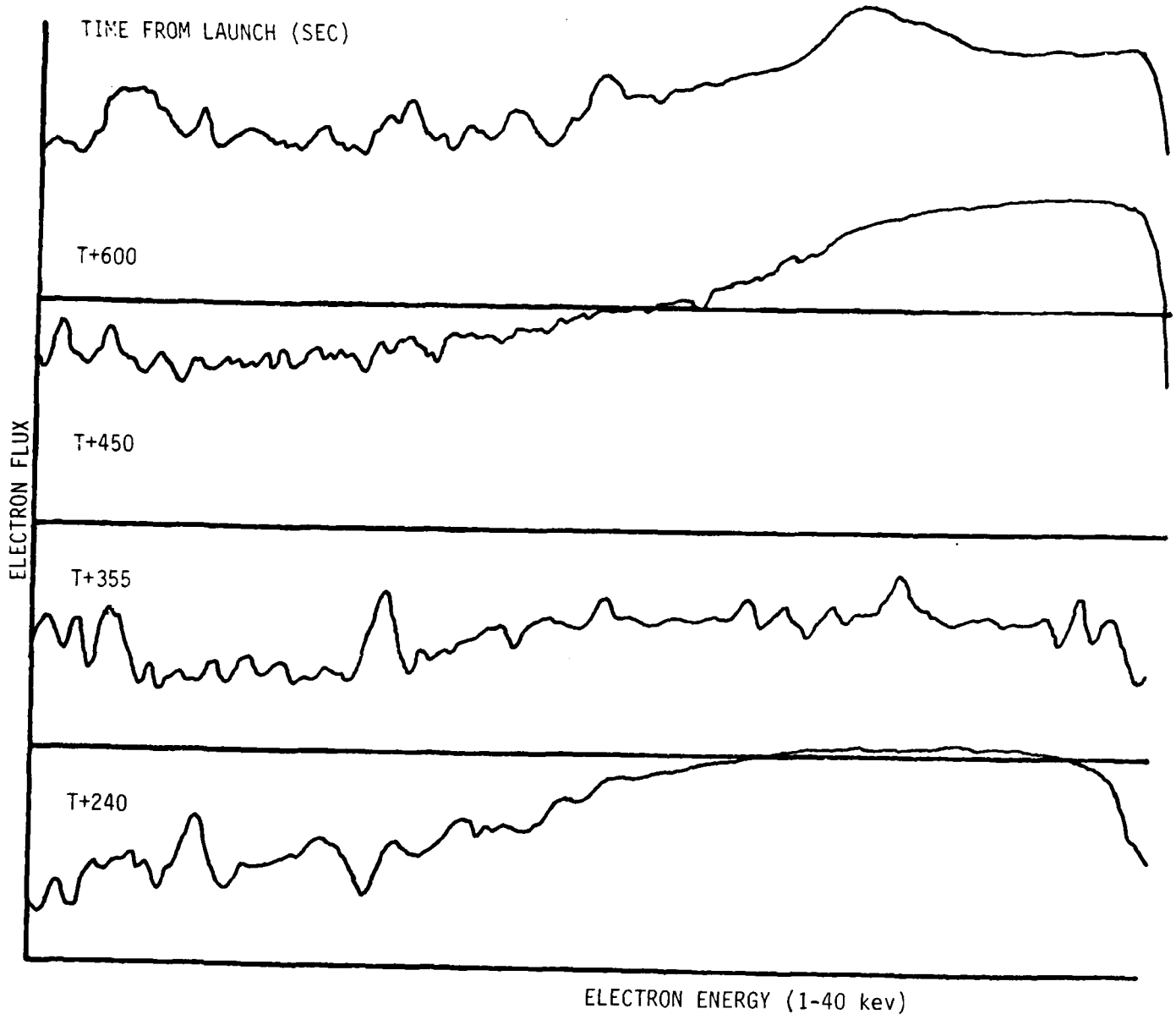

FIGURE 4.18 ROCKET IC819.08-1 ELECTROSTATIC ANALYZER DATA

5.0 ADVANCED ENERGY DEPOSITION SYSTEM

5.1 Introduction

The EXCEDE program was undertaken to provide in situ measurements of an atmosphere perturbed by a controlled energy deposition at levels greatly in excess of natural levels. For this application, we have attempted to evaluate the relative merits of electron guns, ion guns, pulsed and DC operation, and the feasibility of depositing a neutral plasma to eliminate the effects of space charge. The selection of a specific energy deposition source will be affected to a large degree by the problem under study. For instance, the behavior of long-lived F region ionization such as that produced by VUV fireballs can best be simulated with an ion source while E region phenomena can be simulated with an electron beam. Figure 5.1 illustrates the range of protons, electron, photons, and alpha particles as a function of particle energy[8,9]. By combining this with atmospheric density such as shown in Figure 5.2, one can obtain values for the linear range of particles as a function of energy and altitude.

In general, an electron source is the simplest and for this reason it will probably be chosen for most applications. The choice of DC or pulsed operation again will depend on the application. Deposition of a neutral plasma will eliminate spacecraft charge-up. However, to date spacecraft change-up has not been a problem.

Visidyne has already developed a rocketborne 3 kilovolt, 30 kilowatt electron gun system[10] which is the highest power system successfully flown to date. This instrumentation was part of a payload launched from the Poker Flat Research Range, Alaska on 13 April 1975. Its innovative design used high current lithium batteries in series to provide the accelerating voltage. The electron gun utilized a lanthanum hexaboride as a nonpoisonable cathode which can be run at a relatively low temperature ($1700^{o}K$) compared to tungsten ($2600^{o}K$). To maintain a clean environment and minimize outgassing in operation, the electron gun was mounted in a stainless steel vacuum chamber pumped by a Vaclon pump. A high voltage vacuum relay was used to provide beam modulators.

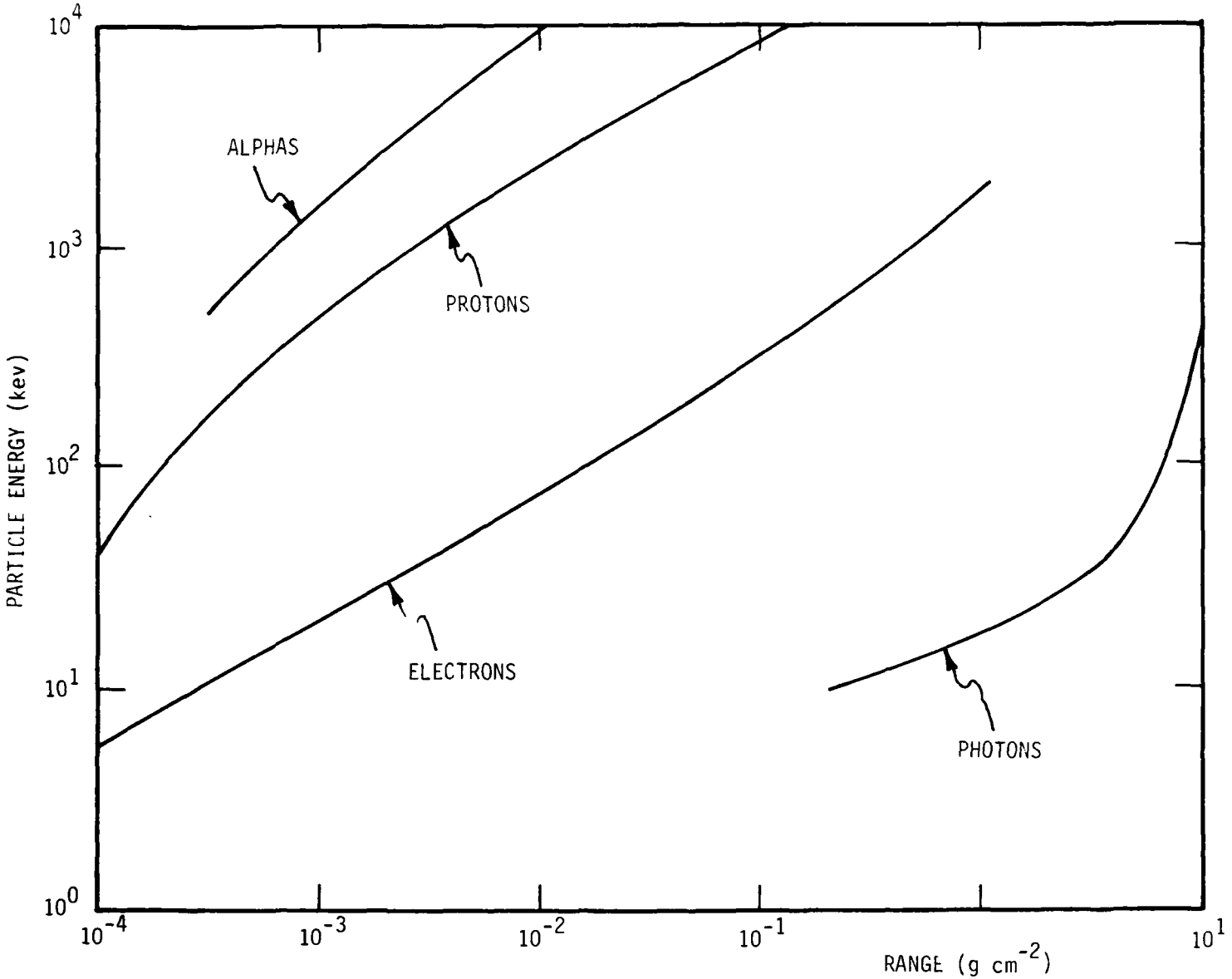

FIGURE 5.1 RANGE OF PARTICLES IN AIR VS. PARTICLE ENERGY

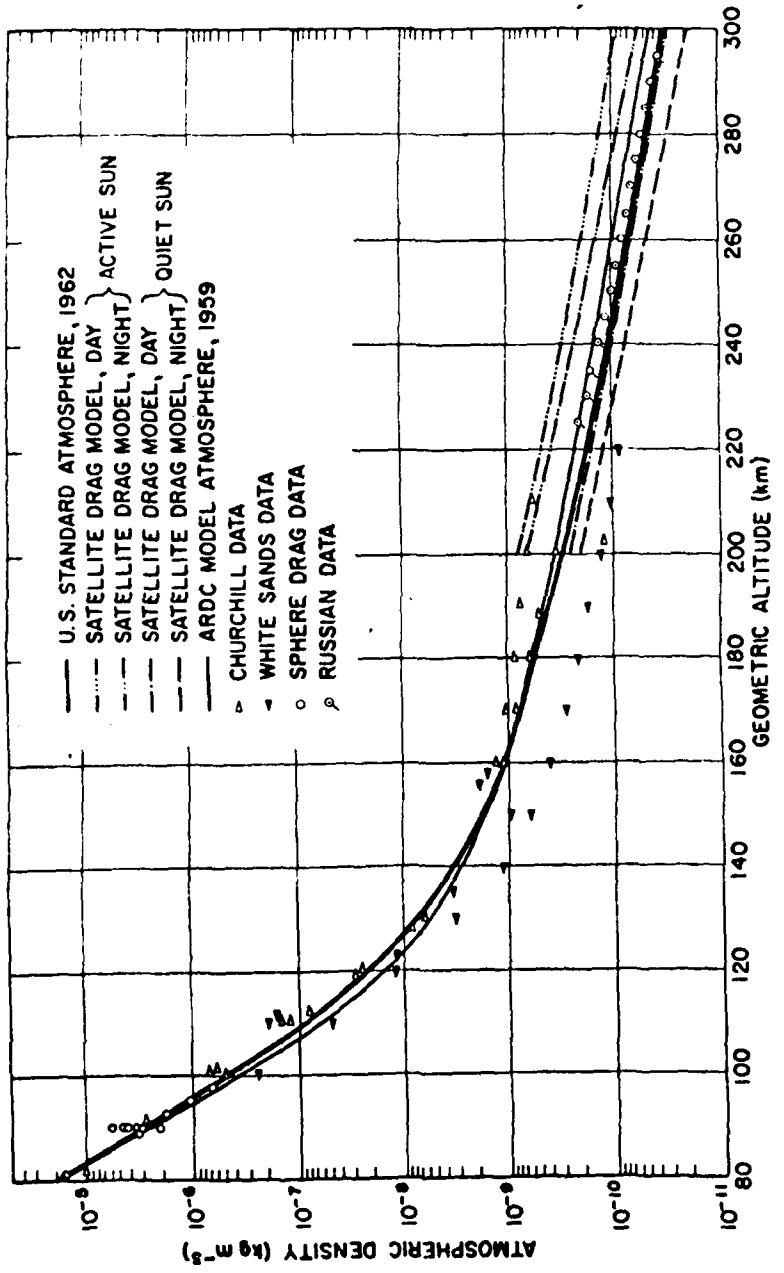

FIGURE 5.2 ATMOSPHERIC DENSITY VS. GEOMETRIC ALTITUDE

5.2 System Design Considerations

The principal limitations today to designing higher power energy deposition systems appear to be space charge near the cathode which limits beam current and the development of a high current DC modulation technique. The theoretical space charge limit on diode current (i_d) is given by:

$$i_d = \frac{2.3 \times 10^{-6} V^{3/2}}{d^2} \quad \frac{amp}{cm^2}$$

The space charge limited current will increase as $V^{3/2}$, but the range of electrons with kilovolt energies is proportional to E^2; therefore, the effect of increasing beam current by increasing beam voltage is to decrease the specific energy depositions.

It is substantially more difficult to design a system to interrupt a DC current than an AC current. In designing a system to interrupt an AC current, one can take advantage of the fact that the current is zero every half cycle. By definition, this condition does not exist for a DC current. In the rocket electron gun system built by Visidyne, a high voltage vacuum relay was used to modulate the beam. This device makes use of the high dielectric strength of high vacuum (10^{-8} torr) and uses high temperature materials (tungsten and molybdenum) for contacts. When a high voltage, high current circuit is switched, an arc will form. In a vacuum relay, this arc will blow out which will further pump the vacuum relay.

Contact bounce is minimized (~½ msec) to reduce the amount of arcing and the rise time (~10^{-7} sec) of the modulated electron beam will be limited only by the lumped circuit parameters. However, a high frequency modulation of the leading edge can occur due to contact bounce.

Lithium batteries have a relatively high internal impedance which limits the short circuit current. In the system under discussion, the short circuit current was 12 amperes. While substantially less than the current that would be generated with other battery systems (An equivalent Ni-Cd battery system would have had a short circuit current in excess of

80 amperes.), this current is still substantial and was beyond the rated load of the high vacuum switch.

Emphasis in our effort was devoted to the development of a technique to reduce space charge effects and to provide a new modulation technique for higher power systems. Possible switching techniques considered included the following:

Fused Switch

One method of protecting the battery supply during E-gun operation would be to use a fused switch. This would consist of a number (~12) of standard high voltage aircraft fuses connected to the contacts of a 12-position motor driven high voltage switch. E-gun beam modulation would be done using a standard high voltage relay. Should a fault occur, the high voltage fuse would immediately blow open, interrupting the E-gun circuit. A sensing circuit would detect a high voltage drop across the open fuse and after a preset time delay, open the modulator switch, then activate the fuse switch drive motor to switch to a new fuse into the circuit. The advantage of this method is that it is done with standard tested components and requires no additional development. The main disadvantage is that only a limited number of circuit faults can be interrupted during a flight.

Switch Gear Contactor

A method which would permit a greater number of fault interrupting would be to use a commercial power line switch-gear contactor. A vacuum bottle type (similar to, but larger than, a high voltage vacuum relay) could be used to modulate and fault interrupt the E-gun circuit. The major problem would be that there are no standard systems available which can be used in this particular application. To obtain a flight qualified, reliable, compact modulator/fault interrupter would require additional engineering and testing.

Additional Techniques

Another possible alternative beam modulation switch is a developmental device, a crossed field switch. This is a gas discharge controlled

switch capable of interrupting large currents. Still other possible switching techniques are to use stacked silicone controlled rectifiers (SCR) in a forced commutation mode of operation and forced commutation of a vacuum switch.

5.3 Virtual Triode Modulation

The essence of this technique is to modulate the anode of the electron gun in the same manner as one would modulate the grid of a conventional triode. Using this technique, one can reduce the interruption current by approximately a factor of twenty, which is the measured ratio of beam to anode current. In addition, by running the gun anode positive with respect to both the gun cathode and the skin the diode space-charge limit can be exceeded. For these reasons, we have chosen virtual triode modulation for the design of the Advanced Energy Deposition System (AEDS).

5.3.1 Operation Techniques

Measurements on the EXCEDE II Test accelerator indicated the following:

a. E-gun anode interception current was typically 300 ma.
b. The E-gun beam return current path was through the payload skin rather than the E-gun anode.
c. The E-gun beam extraction is done by the anode.

Thus, if the E-gun were maintained at high negative voltage and the E-gun anode switched to payload skin potential (~ground), beam emission would result, but the current through the modulator switch would be only on the order of 300 ma. When the anode was switched to cathode potential (high voltage), the E-gun beam would be cut off. Full cutoff could be obtained by biasing the anode slightly negative with respect to the cathode.

The advantage of this modulation technique is that much higher gun current can be modulated without having to develop a new beam switching technique. The disadvantage is that E-gun mechanical mounting becomes more complex, because now the anode must be high voltage isolated from the payload and still be connected to a high capacity thermal sink.

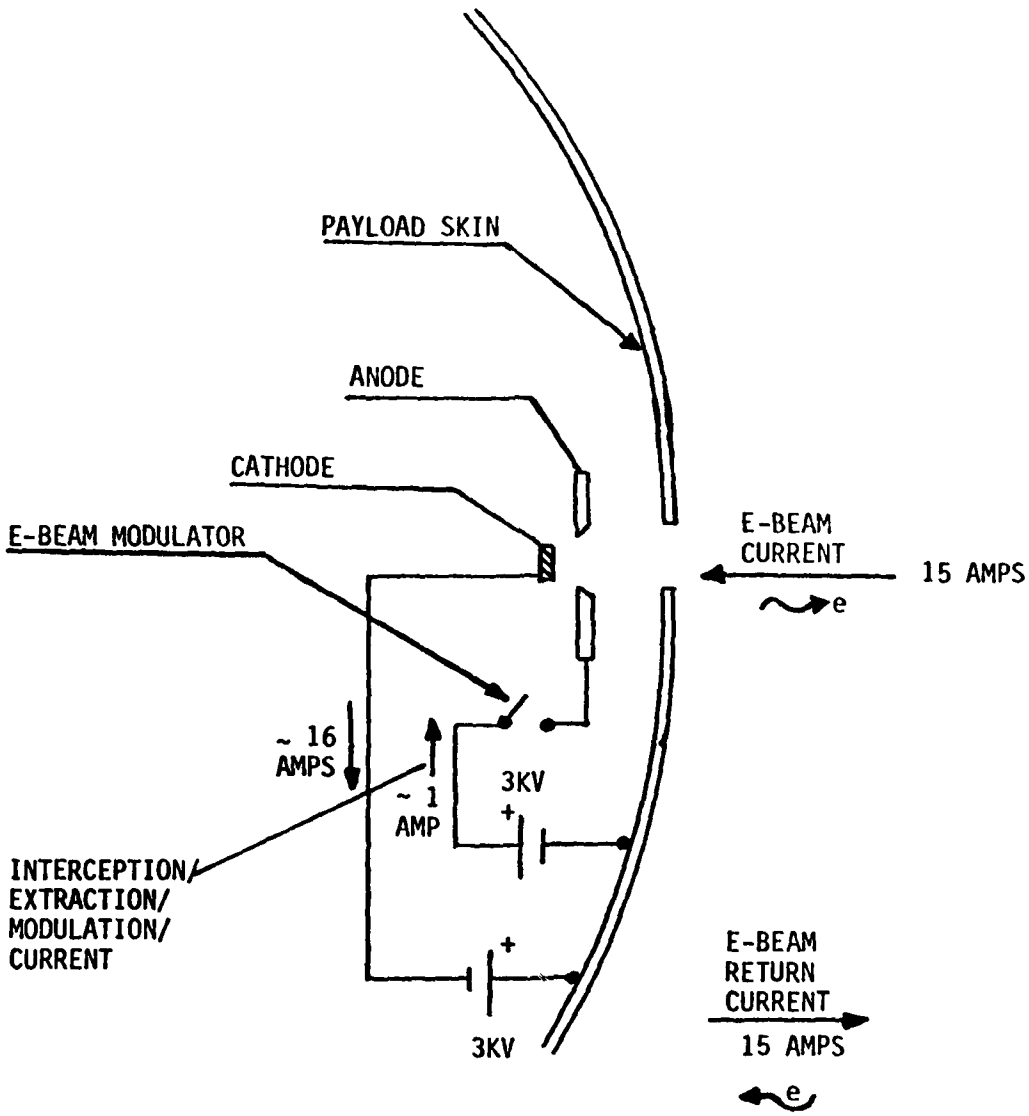

FIGURE 5.3 E-GUN VIRTUAL TRIODE OPERATION

By operating the E-gun in the virtual triode configuration, it may be possible to use the anode as an extraction grid. If the anode-cathode potential were 6 kv, the E-gun perveance limited beam current would be approximately 14 amps. If the E-gun anode is biased as shown in Figure 5.3, then a 14 amp beam current of 3 kev electrons could be emitted. The E-beam emittance angle of the beam would be increased, but for the EXCEDE application, this would not be a problem. It should be noted that only the anode interception current (< 1 amp) is required from the extraction power supply. Thus, a current increase of a factor of three at 3 kv may be possible merely by modifying the E-gun operating anode.

After consideration of the various alternatives, the virtual triode was selected as the most promising concept. It requires only limited new development while offering the possibility of an order of magnitude increase in current capacity. As mentioned above, it also has a result in an increase in current for a given accelerartion potential. A prototype virtual triode system has been assembled and laboratory measurements obtained. These are discussed in Section 5.3.2.

5.3.2 Laboratory Results

An electron gun identical to the type used in the EXCEDE II Test experiment was mounted in a vacuum chamber and connected as shown in Figure 5.3. Acting as a collector in place of the payload skin was a stainless steel plate measuring 9x5 x 0.25 inches and spaced 1.75 inches from the anode. Because of current limitations of the equipment, the maximum anode voltage that could be applied was 1 kv.

The first technique to be examined was that of using the anode as an extraction grid to increase the E-gun beam current. Figure 5.4 showns that with the anode and the collector at the same potential (extraction voltage equal to zero), the perveance of the test gun was essentially the same as those used in the EXCEDE II Test experiment.[10] However, contrary to expectations, operating the E-gun with extraction voltages greater than the beam voltage resulted in somewhat decreased beam currents as can be seen in Figure 5.4. The most likely explanation for this is that secondary electrons are produced at the collector and returned to the anode. As the anode volt-

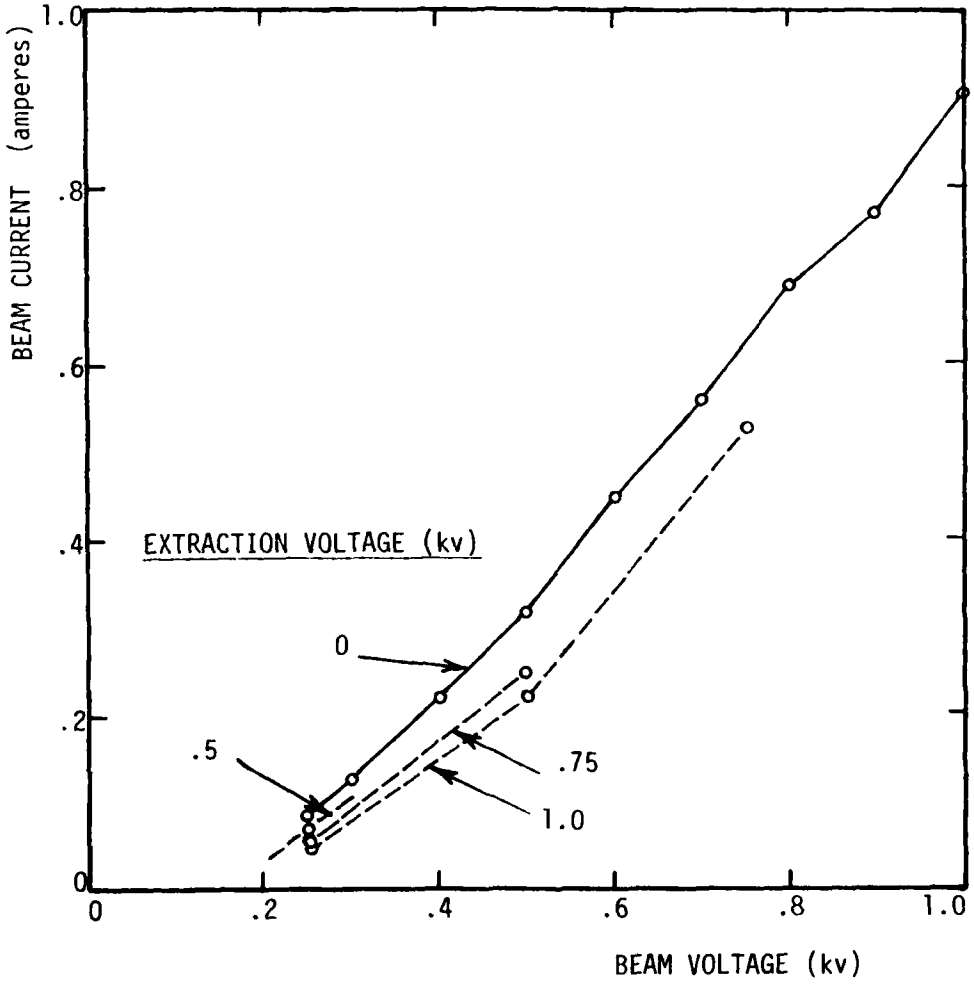

FIGURE 5.4 EFFECT OF EXTRACTION VOLTAGE ON THE E-GUN BEAM

age was increased, the anode current would increase markedly while the beam current would decrease slightly. The conclusion is that to test this technique adequately, it would be necessary to redesign the electron gun.

The second technique to be tested with this prototype system was modulation of the electron beam by using the anode as an extraction grid and biasing it slightly negative with respect to the cathode. The advantage of this technique is that the modulation current to be switched would be an order of magnitude lower than that of the EXCEDE II Test. For this experiment, the E-gun was connected as in Figure 5.5 and the modulation voltage varied from -600 to +600 volts. The results are given in Figure 5.6. They show that the electron beam is completely cut off when the anode voltage is biased negatively at more than 200 volts. This modulation technique, therefore, has successfully been demonstrated. It overcomes one of the principal limitations of designing higher power energy deposition systems, as mentioned in Section 5.2. Its adoption into the design of future EXCEDE experiments is highly recommended.

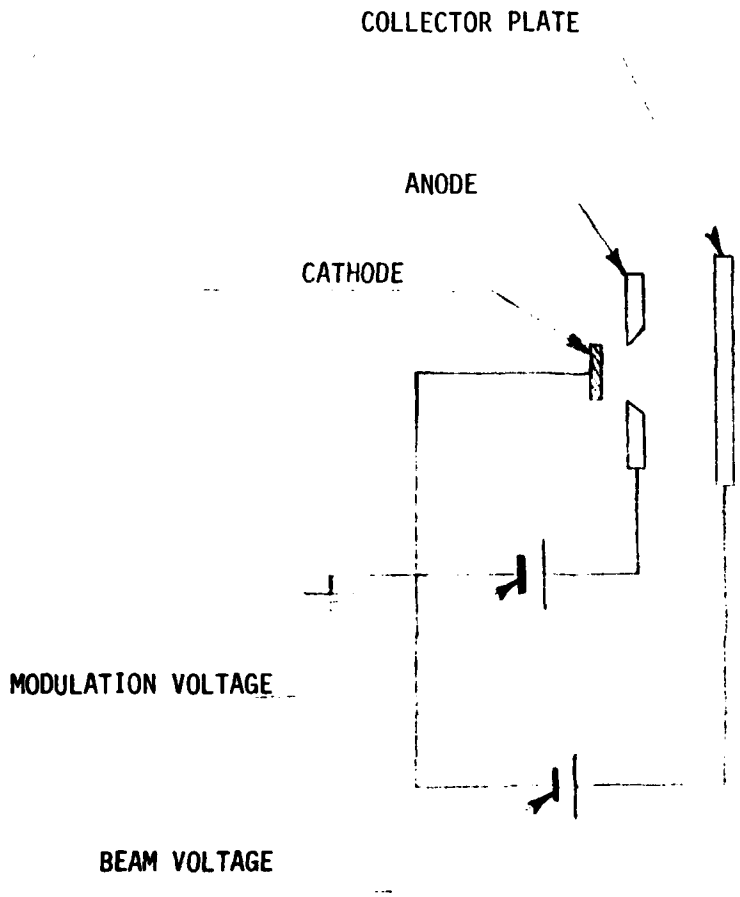

FIGURE 5.5 E-GUN BEAM MODULATION EXPERIMENT

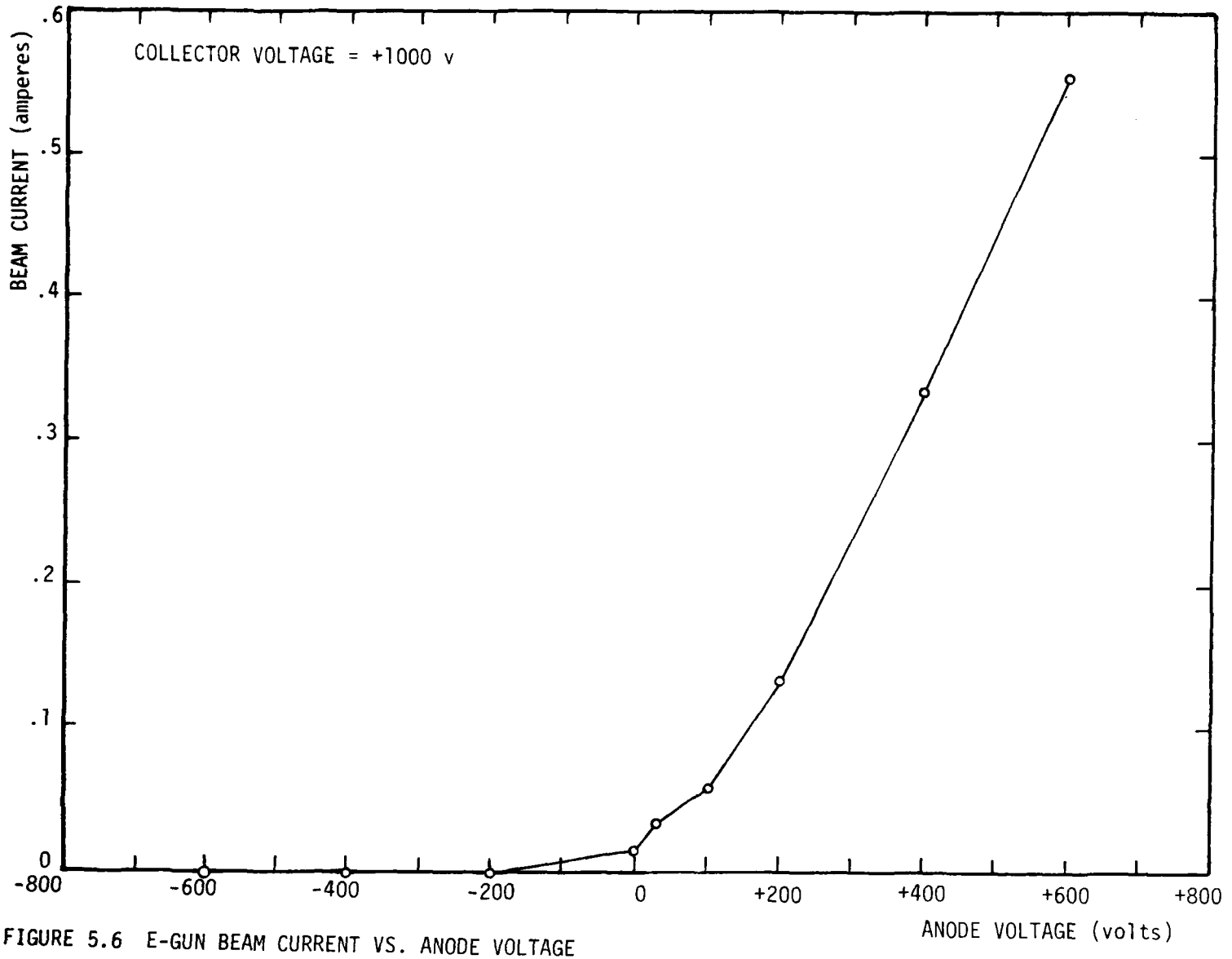

FIGURE 5.6 E-GUN BEAM CURRENT VS. ANODE VOLTAGE

6.0 REFERENCES

1. Reidy, W.P., G. Aurilio, R.W. Brooke, S. Rappaport, O. Shepherd, and T.F. Zehnpfennig, "The Balloon Altitude Mosaic Measurements (BAMM) Program and Laboratory Studies of an Infrared Background Optical Suppression Scheme (BOSS), VI-500, Visidyne, Inc., Scientific Report No. 4, Contract No. F19628-76-C-0198, 1 December 1978.

2. Brooke, R.W., O. Shepherd, G. Aurilio, R.D. Bucknam, and W.H. Sheehan, "Balloon-Borne Gondola for BAMM", VI-460, Visidyne, Inc., BAMM Report No. 5, Contract No. F19628-76-C-0198 (to be published as an AFGL Technical Report).

3. Shepherd, O., W.P. Reidy, T.F. Zehnpfennig, G.A. Vanasse, and A.T. Stair, Jr., "IR Background Suppression Studies", VI-382A, Visidyne, Inc., Scientific Report No. 1, Contract No. F19628-76-C-0198, AFGL-TR-77-0277, May 1977.

4. Huppi, R.J. and J.W. Reed, "Aircraft Borne Measurements of Infrared Enhancements During ICECAP 1975 and 1976", USU, AFGL-TR-77-0232, HAES Report No. 68, September 1977.

5. Sternglass, E.J., "Backscattering of Kilovolt Electrons from Solids", Phys. Rev., 95, 345 (1954).

6. Katz L., and A.S. Penfeld, Rev. Mod. Phys., 74, 28 (1952).

7. Menefee, J., C.F. Swinehart, and E.W. O'Dell, "Calcium Fluoride as an X-ray and Charged Particle Detector", IEEE Trans. Nucl. Sci., NS-13, 720 (1966).

8. Cladis, J.B., G.T. Davidson, and L.L. Newkirk, "The Trapped Radiation Handbook", Lockheed Palo Alto Research Laboratory, DNA 2524H, Contract No. DNA 001-73-C-0065, January 1977.

9. Evans, R.D., "The Atomic Nucleus", McGraw-Hill, New York (1955).

10. Shepherd, O., J.W. Carpenter, W.P. Reidy, W.H. Sheehan, and T.F. Zehnpfennig, "The Design and Flight Test of a 30 kw Rocketborne Electron Accelerator Module (EXCEDE II Test), HAES Report No. 22, AFCRL-TR-75-0379, VI-289, Visidyne, Inc., July 1975.

DISTRIBUTION LIST

DEPARTMENT OF DEFENSE

Director
Defense Advanced Rsch. Proj. Agency
Attn: LTC W.A. Whitaker

Director
Defense Nuclear Agency
Attn: TITL Tech. Library (3 copies
Attn: TISI Archives
Attn: RAEV Harold C. Fitz, Jr.
Attn: RAAE Lt/Col. McKechney
Attn: RAAE Capt. Peter Lund
Attn: RAAE Dr. Patrick Crowley

Dir. of Defense Rsch. & Engineering
Department of Defense
Attn: DD/S&SS (OS) Daniel Brockway

Commander
Field Command
Defense Nuclear Agency
Attn: FCPR

Chief Livermore Division
FLD Command DNA
Attn: FCPRL

DEPARTMENT OF THE ARMY

Commander/Director
Atmospheric Sciences Laboratory
U.S. Army Electronics Command
Attn: DRSEL-BL-SY-A.F. Niles
Attn: H. Ballard

Commander
Harry Diamond Laboratories
Attn: DRXDO-NP, F.H. Wiminetz
(2 Copies)

[illegible]
[illegible] Post Graduate School
Attn: Rsch Rpts Librarian

[illegible]
[illegible] Intelligence Support Center
[illegible] Document Control

Director
BMD Advanced Technical Center
Attn: ATC-T, M. Capps
Attn: ATC-O, M. Davies

Dep. Chief of Staff for Rsch. Dev & Accout.
Department of the Army
Attn: MCB Division
Attn: DAMA-CSZ-C
Attn: DAMA-WSZC

Director
U.S. Army Ballistic Rsch. Labs.
Attn: John Mester
Attn: Tech. Library

Commander
U.S. Army Electronics Command
Attn: Inst. for Expl. Research
Attn: Weapons Effects Section

Commander
CORADCOM
Attn: PP-Library
Attn: DRDCO-COM-D

DEPARTMENT OF THE NAVY

Commander
Naval Oceans Systems Center
Attn: Code 2200 William Moler

Director
Naval Research Laboratory
Attn: Code 7712 D.P. McNut
Attn: Code 6701 J.D. Brown
Attn: Code 2600 Tech. Library
Attn: Code 7175J C.Y. Johnson
Attn: Code 6700 T.P. Coffey
Attn: Code 7709 Wahab Ali
Attn: Code 6780 D.F. Strobel
Attn: Code 6780 P. Juluenne
Attn: Code 67800 J. Fedder
Attn: Code 6780 S. Ossakow
Attn: Code 6707 J. Davis

Commander
Naval Surface Weapons Center
Attn: Code WA 501 Navy NUC
Programs Office
Attn: Technical Library

DEPARTMENT OF THE AIR FORCE

AF Geophysics Laboratory, AFSC
Attn: LKB, K.S.W. Champion
Attn: OPR, A.T. Stair, Jr.
Attn: OPR, P.G. Doyle
Attn: OPR, R. Murphy
Attn: LKO, R. Huffman
Attn: OPR, J. Kennealy

AF Weapons Laboratory, AFSC
Attn: Maj. Gary Ganong, DES

Commander
ASD
Attn: ASD-YH-EX-LTC R. Leverette

SAMSO/AW
Attn: SZJ Lt. Col. Doan

SAMSO/YN
Attn: Maj. P. Sivgals

AFTAC
Attn: Tech Library
Attn: TD

HQ
Air Force Systems Command
Attn: DLS
Attn: Tech Library
Attn: DLCAE
Attn: DLTW
Attn: DLXP
Attn: SDR
Attn: RDQ

US ENERGY RSCH. AND DEV. ADMIN

Division of Military Application
U.S. Energy Rsch. & Dev. Admin.
Attn: DOC CON

Los Alamos Scientific Laboratory
Attn: DOC CON for H.V. Argo
Attn: DOC CON for M.B. Pongratz
Attn: DOC CON for R. Brownlee
Attn: Group AP-4, MS 567
Attn: DOC CON for J. Zinn

University of California
Los Alamos Scientific Laboratory
Attn: Librarian MS 362

Sandia Laboratories
Attn: DOC CON for W.B. Brown, Org. 1353
Attn: Tech Library Org. 3141

Argonne National Laboratory
Records Control
Attn: DOC CON for D.W. Green
Attn: DOC CON for LIR SVCS Rpts Sec.
Attn: DON CON for G.T. Reedy

University of California
Lawrence Livermore Laboratory
Attn: W.H. Duewer, L-262
Attn: J. Chang, L-71

U.S. Energy Rsch. & Dev. Administration
Division of Headquarters Services,
Library Branch
Attn: DOC CON for Class. Tech. Library

OTHER GOVERNMENT

Department of Transportation
Office of the Secretary
Attn: S.C. Coroniti

NASA
Langley Station
Attn: Tech. Library

NASA
Ames Research Center
Attn: N-245-3 R. Whitten

Department of the Army
Bal. Missl. Def. Adv. Tech. Ctr.
Attn: W.O. Davies

Federal Aviation Administration
Attn: HAPP/AEQ-10/James W. Rogers

Central Intelligence Agency
Attn: ED/SI RM 5G48 HQ Bldg.
Attn: NED/OS I-2G4R HQS

Department of Commerce
National Bureau of Standards
Attn: Sec. Officer for M. Krauss
Attn: Sec. Off. for L.H. Gevantman

National Oceanic & Atmospheric Admin.
Environmental Research Laboratories
Department of Commerce
Attn: G. Reid
Attn: E. Ferguson
Attn: F. Fehsenfeld

DEPARTMENT OF DEFENSE CONTRACTORS

Science Applications, Inc.
Attn: D.G. Hopper

Aero-Chem Research Laboratories, Inc.
Attn: A. Fontign
Attn: H. Pergament

Aerodyne Research, Inc.
Attn: F. Bien
Attn: M. Camac

Aerospace Corporation
Attn: N. Cohen
Attn: H. Mayer
Attn: R.J. McNeal
Attn: T.D. Taylor
Attn: J. Reinheimer
Attn: R.D. Rawcliffe
Attn: R. Herm

Battelle Memorial Institute
Attn: H.L. LaMuth
Attn: STOIAC

Brown Engineering Company, Inc.
Attn: N. Passino

General Research Corporation
Attn: D. Jones
Attn: J. Ise, Jr.

California At Riverside, University of
Attn: J.N. Pitts, Jr.
Attn: A.M. Winer

California At San Diego, University of
Attn: S.C. Lin

California University of Berkley
Attn: Sec. Off. for H. Johnston
Attn: Sec. Officer for Dept of Chem., H.L. Strauss

Calspan Corporation
Attn: C.E. Treanor
Attn: J.M. Grace
Attn: M.G. Dunn
Attn: W. Wruster

University of Colorado
Astro-Geophysics
Attn: J.B. Pearce

Colorado, University of
Office of Contracts and Grants
Attn: G.M. Lawrence, LASP

Concord Sciences
Attn: E.A. Sutton

University of Denver
Space Science Laboratory
Attn: B. Van Zyl

University of Denver
Denver Research Laboratory
Attn: Sec Officer for D. Murcray

AVCO-Everett Research Laboratory Inc.
Attn: Tech. Library
Attn: C.W. Von Rosenberg, Jr.

General Electric Company
Space Division
Attn: M.H. Bortner, Space Sci. Lab
Attn: J. Burns
Attn: F. Alyea
Attn: P. Zavitsands
Attn: R.H. Edsall
Attn: T. Baurer

Geophysical Institute
University of Alaska
Attn: J.S. Wagner

Lowell University of
Center for Atmospheric Research
Attn: G.T. Best

Lockheed Missiles and Space Company
Attn: J. Kumer, Dept 52-54
Attn: J.B. Cladis, Dept 52-12, B202
Attn: B.M. McCormac, Dept 52-54
Attn: T. James, Dept 52-54
Attn: M. Walt, Dept 52-10
Attn: R.D. Sears, Dept 52-54

Institute for Defense Analysis
Attn: E. Bauer
Attn: H. Wolfhard

Mission Research Corporation
Attn: D. Archer
Attn: D. Fischer
Attn: M. Scheibe
Attn: D. Sappenfield
Attn: D. Sowle

Photometrics, Inc.
Attn: I.L. Kofsky

Berkeley Research Associates
Attn: J.B. Workman

Physical Dynamics, Inc.
Attn: A. Thomas

General Electric Company
Tempo-Center for Advanced Studies
Attn: DASAIC
Attn: W.S. Knapp
Attn: T. Stephens
Attn: D. Chandler
Attn: V.R. Strull

Physics International Company
Attn: DOC CON for Tech Library

Pittsburg, University of the Comwlth
System of Higher Education
Attn: W.L. Fite
Attn: M.A. Biondi
Attn: F. Kaufman

R&D Associates
Attn: R. Latter
Attn: R.G. Lindgren
Attn: B. Gabbard
Attn: R. Lelevier
Attn: A.L. Latter
Attn: F. Gilmore
Attn: H.J. Mitchell

Rand Corporation
Attn: C. Crain

Science Applications, Inc.
Attn: D.A. Hamlin
Attn: D. Sachs
Attn: D.G. Hopper

Stanford Research Institute International
Attn: M. Baron
Attn: W.G. Chesnut

Technology International Corporation
Attn: W.P. Boquist

United Technologies Corporation
Attn: R.H. Bullis

Utah State University
Attn: D. Baker
Attn: K. Baker
Attn: C. Wyatt
Attn: A. Steed

Physical Science, Inc.
Attn: K. Wray
Attn: R.L. Taylor
Attn: G. Caledonia

Commander
Rome Air Development Center
Attn: OSCA, J.J. Simons
Attn: OSCA, J.J. Simons

Steward Radiance Laboratory
Attn: R. Huppi

Boston College
Space Data Analysis Laboratory
Attn: E.R. Hegblom
Attn: W.F. Grieder

Forrestial Campus Library
Princeton University
Attn: Librarian

Visidyne, Inc.
Attn: H. Smith
Attn: J.W. Carpenter
Attn: T.C. Degges
Attn: C. Humphrey
Attn: W.P. Reidy

Wayne State University
Attn: R.H. Kummler
Attn: W.E. Kaupplia

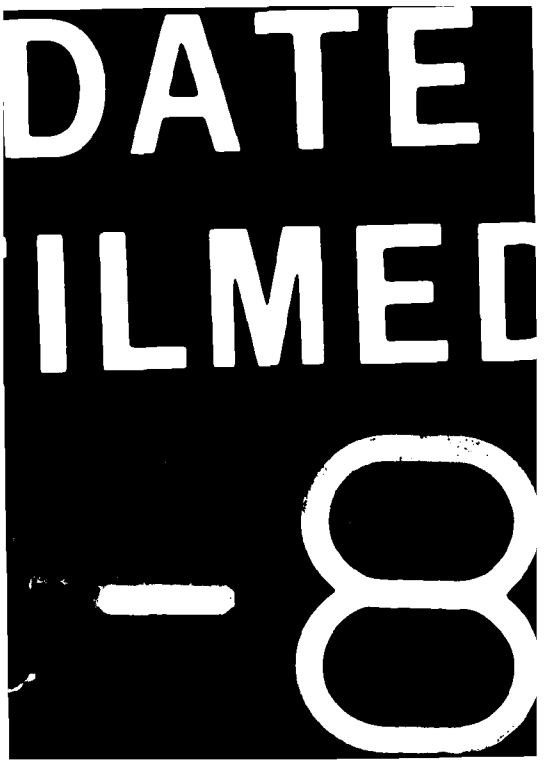
DATE
ILMED
8